UNIVERSITY OF CALIFORNIA SAN DIEGO

Lamin B1 mediates nuclear integrity and chromatin organization

A dissertation submitted in partial satisfaction of
the requirements for the degree Doctor of Philosophy

in

Biology

by

Jeanae M. Kaneshiro

Committee in charge:

Professor Martin W. Hetzer, Chair
Professor Arshad Desai
Professor Anthony Hunter
Professor Jens Lykke-Andersen
Professor Deborah Yelon

2021

The Dissertation of Jeanae M. Kaneshiro is approved, and it is acceptable in quality and form for publication on microfilm and electronically.

University of California San Diego

2021

TABLE OF CONTENTS

LIST OF FIGURES

LIST OF TABLES

ACKNOWLEDGEMENTS

I would first like to thank my advisor, Martin W. Hetzer, for all of his support throughout my years in graduate school. His positivity helped me to persevere through the tough times, and I am very grateful that I had the opportunity to complete my dissertation in his laboratory.

I would also like to thank my committee members, Arshad Desai, Tony Hunter, Jens Lykke-Andersen, and Deborah Yelon, for always setting aside time to meet with me, and for giving me constructive feedback and encouraging words throughout graduate school.

I am very grateful for all of the members of the Hetzer lab for generously sharing their time and expertise, and for making lab enjoyable each and every day. I would specifically like to acknowledge Abigail Buchwalter, who mentored me during my rotation and throughout my early years in graduate school. She is an inspiring scientist, and one I have learned so much from. I would also like to recognize Juliana S. Capitanio, who has been instrumental in moving my projects forward and who has always provided me with critical advice on my research. Last, and most definitely least, I would like to thank my BFF, Brandon H. Toyama, for always pushing me to be my best.

Chapter 2 is unpublished material coauthored with Buchwalter, Abigail and Capitanio, Juliana S. The dissertation author, under guidance of Martin W. Hetzer, was the primary researcher and author of this material.

Chapter 3 is unpublished material coauthored with Capitanio, Juliana S. The dissertation author, under guidance of Martin W. Hetzer, was the primary researcher and author of this material.

Chapter 4, in full, is currently being prepared for submission for publication. Kaneshiro, Jeanae M.; Capitanio, Juliana S.; Hetzer, Martin W. The dissertation author, under guidance of Martin W. Hetzer, was the primary researcher and author of this material.

VITA

2014	Bachelor of Science, University of Notre Dame
2021	Doctor of Philosophy, University of California San Diego

PUBLICATIONS

Buchwalter, A., **Kaneshiro, J. M.**, & Hetzer, M. W. Coaching from the sidelines: the nuclear periphery in genome regulation. *Nat Rev Genet.* **20**:39-50 (2019).

ABSTRACT OF THE DISSERTATION

Lamin B1 mediates nuclear integrity and chromatin organization

by

Jeanae M. Kaneshiro

Doctor of Philosophy in Biology

University of California San Diego, 2021

Professor Martin W. Hetzer, Chair

The nuclear envelope (NE) is associated with two major protein complexes: nuclear pore complexes (NPCs) and the nuclear lamina. NPCs are ~120 MDa structures that perforate the NE and mediate nucleocytoplasmic transport, and the nuclear lamina is a network of type V intermediate filaments that forms a meshwork lining the nucleoplasmic side of the inner nuclear membrane (INM) and provides structure to the nucleus. Aside from these canonical functions of NPCs and the nuclear lamina, it has been discovered that these complexes and their

subcomponents have additional roles, such as those in chromatin organization and gene regulation. This dissertation aims to expand the known functions of proteins within these complexes, and focuses on two NPC components, Nup98 and Nup96 (Nup98/96), and the lamin isoform, Lamin B1 (LmnB1).

Chapter 2 suggests a novel function for Nup98/96 in maintaining the integrity of the nuclear lamina. Small interfering RNA (siRNA) mediated knockdown (KD) of Nup98/96 enlarges the lamina meshwork across the nuclear surface and increases the frequency of transient nuclear envelope rupture. This weakening of the nuclear lamina was further determined to be a consequence of reduced LmnB1 expression, and Chapter 3 shows that LmnB1 is post-transcriptionally regulated through its 3' untranslated region upon Nup98/96 KD. However, further analysis indicated that the siRNA oligonucleotides designed against Nup98/96 also target LmnB1 for degradation. These siRNAs mimicked microRNAs, hsa-miR-218 and hsa-miR-636, through sequence similarities within their seed regions, allowing these siRNAs to directly target LmnB1. Therefore, Nup98/96 does not regulate the nuclear lamina through LmnB1, and the ability of siRNAs to mimic miRNAs should be carefully considered when designing and utilizing siRNAs in future studies.

Chapter 4 describes the effects of LmnB1 overexpression (OE) on chromatin organization and senescence induction. LmnB1 OE induces the formation of heterochromatic DNA foci within the nucleoplasm, coinciding with a reduction of heterochromatin at the nuclear periphery. This leads to changes in gene expression, which may be a consequence of altered chromatin accessibility or changes in histone modifications. The release of heterochromatin from the nuclear periphery is not a consequence of reducing other NE proteins, such as Lamin A or lamin B receptor, that are important for tethering heterochromatin at the nuclear periphery. This

suggests that LmnB1 OE might increase the thickness of the nuclear lamina and disrupt the binding of heterochromatin tethers at the nuclear periphery. Finally, although the induced heterochromatin foci are reminiscent of the DNA organization described in senescent cells, LmnB1 OE slows cell proliferation but does not induce senescence.

Overall, this dissertation demonstrates the importance of tightly regulating LmnB1 expression to maintain nuclear integrity and chromatin organization. Several human diseases show misregulation of LmnB1, and an interesting observation is the increased expression of LmnB1 observed in various types of cancer, some of which also correlate with higher tumor grade and poor prognosis. This suggests that LmnB1 OE might promote tumorigenesis, which may be mediated through changes in chromatin organization and gene expression, as shown in Chapter 4. However, given the reduction in cell proliferation that was also observed upon LmnB1 OE, further mechanistic studies will be required to reconcile whether LmnB1 OE may be pro-tumorigenic or tumor suppressive.

Chapter 1: Introduction

The Nuclear Pore Complex

NPC structure and function

The nuclear pore complex (NPC) is an ~120 MDa structure that perforates the nuclear envelope (NE) and mediates transport between the nucleus and the cytoplasm. NPCs are composed of ~30 different proteins called nucleoporins (Nups) that are further classified as scaffold Nups or peripheral Nups, based on their location, dynamics, and function (Beck and Hurt, 2017). Scaffold Nups provide the structural framework for the NPC and are located within the inner core. These Nups are essential for NPC assembly, and remain stably associated with the NPC with limited protein exchange (Belgareh *et al.,* 2001; Harel *et al.,* 2003; Rabut *et al.,* 2004; Toyama *et al.,* 2013). Peripheral Nups form the cytoplasmic filaments and nuclear basket of the NPC. These Nups function in transporting cargo across the NPC and can dynamically shuttle on and off the pore (van Deursen *et al.,* 1996: Wu *et al.,* 2001; Rabut *et al.,* 2004).

NPCs regulate gene expression

Although NPC function in nucleocytoplasmic transport has been well established, recent advances in the field have demonstrated the importance of NPCs and individual Nups in modulating gene expression. NPCs have been shown to activate gene expression by interacting with enhancers and super enhancers (SEs) within the genome (Pasqual-Garcia *et al.,* 2017, Ibarra *et al.,* 2016). Enhancers are regulatory elements in the DNA that bind transcription factors to promote gene expression, and SEs are defined as multiple enhancers clustered together (Pott and Lieb, 2015). Of the Nups comprising the NPC, Nup98, Nup93, and Nup153 have been identified as gene activators. Nup98 mediates long-range genome interactions between enhancers and

promoters at the nuclear periphery in *Drosophila melanogaster* for transcriptional memory and proper gene reactivation (Pasqual-Garcia *et, al.,* 2017). Nup93 and Nup153 interact with specific SEs in human cells to activate transcription of SE associated genes in a cell type specific manner (Ibarra *et al.,* 2016).

NPCs also function in gene repression by recruiting chromatin regulators to specific genomic loci. Nup170p, the yeast homologue of Nup155, functions in transcriptional repression of ribosomal genes and subtelomeric DNA by facilitating the interaction between these regions of the genome and chromosome remodeling complexes (Van de Vosse *et al.,* 2013). Additionally, in mouse embryonic stem cells (ESCs), Nup153 silences early differentiation genes by binding transcription start sites and recruiting the polycomb-repressive complex 1 (Jacinto *et al.,* 2015).

Nucleoporins regulate transcription within the nucleoplasm

Specific Nups have also been shown to regulate gene expression within the nucleoplasm, as separate entities away from the NPC, including Sec13, Nup50, Nup62, Nup88, and Nup98 (Kalverda *et al.,* 2010; Capelson *et al.,* 2010; Liang *et al.,* 2013; Panda *et al.,* 2014). Nup98 is one of the best characterized Nups functioning in intranuclear gene regulation, and recent studies have begun to identify Nup98 binding proteins critical for its role in transcription.

In *D. melanogaster*, Nup98 binds the methyl binding domain-related 2/nonspecific lethal complex, which regulates transcriptional activation through H4K16 acetylation at promoters (Pasqual-Garcia *et al.,* 2014; Prestel *et al.,* 2010; Raja *et al.,* 2010). This interaction recruits Nup98 to specific promoters, such as Hox genes, and is essential for their transcription during development (Pasqual-Garcia *et al.,* 2014). Nup98 has also been implicated in transcription

activation in hematopoietic progenitor cells through its interaction with the Wdr82-Set1a/COMPASS complex, which deposits H3K4me3 marks at promoters (Franks *et al.,* 2017). RNA helicase DHX9 was also identified as a strong binding partner with Nup98, in HEK293T cells, and this interaction was important for stimulating the ATPase activity of DHX9 to regulate transcription of select genes (Capitanio *et al.,* 2017).

Nucleoporins post-transcriptionally regulate gene expression

NPCs and Nups also regulate gene expression at the post-transcriptional level. mRNA export was the first example of post-transcriptional gene regulation mediated by NPCs (Blobel, 1985; Ullman *et al.,* 1999; Chakraborty *et al.,* 2008). However, recent studies have demonstrated a direct role for Nups in mRNA splicing and stability. In HEK293T cells, Nup98 functions with DHX9 to bind specific mRNA transcripts and regulate their splicing, and in HepG2 cells, Nup98 stabilizes select p53 induced transcripts by binding their 3' untranslated regions (UTRs) and preventing their degradation by the exosome (Capitanio *et al.,* 2017; Singer *et al.,* 2012).

It is not known whether Nup98 can regulate post-transcriptional gene expression through other mechanisms, or if additional Nups can also function in this process. However, the data supporting Nup-mediated post-transcriptional gene regulation, independent of transport, represents an interesting field in Nup biology for further exploration.

Nucleoporin misregulation in cancer

Given the functional breadth of Nups and NPCs, its is not surprising that mutations or altered expression of Nups have been reported in various tumors, and linked to the misregulation of important signaling pathways that are often disrupted in cancer. The p53 pathway is one of the

most commonly misregulated pathways that lead to tumor development, as it is critical for initiating cell cycle arrest, cellular senescence, or apoptosis, when cells encounter a stress signal. Recently, p21 (CDKN1a), an important tumor suppressor gene within the p53 pathway, was shown to be post-transcriptionally regulated by Nup98 in hepatocellular carcinoma (HCC) cell lines. Examination of HCC tissues showed a downregulation of Nup98 expression and a positive correlation with p21 expression, further supporting a regulatory link between Nup98 and the p53 pathway in preventing tumorigenesis (Singer *et al.,* 2012).

Another pathway frequently disrupted in cancer is the Notch signaling pathway, which is important for regulating cell fate. Nup214 and Nup88 were recently identified as negative regulators of Notch signaling by facilitating nuclear export of Notch activator RBP-J, and precluding its binding to Notch target genes. Aberrant Notch signaling is the cause of ~50% of T-cell acute lymphatic leukemia (T-ALL) cases, and interestingly, ~10% of T-ALL cases harbor chromosomal translocations including Nup214. Nup214 fusion proteins were shown to displace or sequester Nup214 away from the NPC and increase Notch signaling, suggesting a mechanism through which Nup214 chromosomal translocations promote tumorigenesis (Kindermann *et al.,* 2019).

These are select examples that clearly demonstrate the functional breadth of Nups and how their misregulation can disrupt critical signaling pathways. It will therefore be important to continue elucidating the various functions of Nups to better understand how their aberrant expression may impact disease progression.

The Nuclear Lamina

Nuclear lamina structure and function

The nuclear lamina is a network of type V intermediate filaments that lines the nucleoplasmic side of the inner nuclear membrane (INM) and provides structure to the nucleus. There are two types of lamin isoforms. A-type lamins include Lamin A (LmnA) and Lamin C (LmnC), which are splice variants of the *LmnA* gene, and B-type lamins include Lamin B1 (LmnB1) and Lamin B2 (LmnB2), that are encoded by the *LmnB1* and *LmnB2* genes, respectively (Aebi *et al.,* 1986; McKeon *et al.,* 1986). These isoforms assemble into individual networks that interconnect to form a stable lamina (Shimi *et al.,* 2015).

The nuclear lamina has been studied extensively, and it functions in many cellular processes, including maintaining nuclear integrity, and scaffolding proteins and chromatin at the nuclear periphery (Vargas *et al.,* 2012; Ivorra *et al.,* 2006; Paddy *et al.,* 1990). Nuclei lacking proper expression of lamin proteins have misshapen nuclei, altered chromatin organization, and increased frequency of transient NE rupture, an event in which the NE is temporarily perturbed, compromising nuclear and cytoplasmic compartmentalization (Sullivan *et al.,* 1999; Vergnes *et al.,* 2004; Shimi *et al.,* 2008; Vargas *et al.,* 2012; Earle *et al.,* 2020). Although the NE is repaired and sorting of nuclear and cytoplasmic components is reestablished in cells that undergo transient NE rupture, some proteins (e.g. transcription factors) and macromolecular complexes (e.g. mitochondria) remain permanently mislocalized, and cells incur DNA damage (Vargas *et al.,* 2012; De Vos *et al.,* 2011; Denais *et al.,* 2016).

Lamin assembly

To ensure nuclear integrity, cells must maintain a properly assembled lamina. During interphase, lamins are imported into the nucleus through NPCs and assemble into the lamina network or within the nucleoplasm (Shimi *et al.,* 2008). However, when cells enter mitosis, the nuclear lamina must disassemble for NE breakdown. This occurs through phosphorylation of lamins by cyclin dependent kinase 1 and protein kinase C (Peter *et al.,* 1990; Goss *et al.,* 1994), allowing LmnA to disperse into the cytoplasm, and LmnB1 and LmnB2, which remain membrane bound through farnesyl lipid anchors, to disassemble and be stored with the endoplasmic reticulum (Moir *et al.,* 2000; Stick *et al.,* 1988). As cells exit mitosis, lamins are dephosphorylated by protein phosphatase 1a and reassembled to form the nuclear lamina (Thompson *et al.,* 1997).

The B-type lamins, particularly LmnB1, are assembled during late anaphase and early telophase and form a stable network by late telophase. However, the A-type lamins require import through NPCs and form a stable network by early G1 (Moir *et al.,* 2000). Of the lamin isoforms, LmnB1 has been shown to have an essential role in seeding the assembly of the nuclear lamina. Depletion of LmnB1 leads to a disruption in the lamina, characterized by enlarged LmnA and LmnB2 meshworks across the nuclear surface. This disruption was not observed when LmnA or LmnB2 were depleted, emphasizing the importance of LmnB1 for lamin assembly (Shimi *et al.,* 2008).

Lamin expression is cell type specific

Lamins have unique expression patterns amongst different cell types and are tightly regulated during differentiation. This is exemplified in the hematopoietic system, which shows

differential expression of lamin isoforms in several mature blood cell types. For example, in T-cells that exit the bone marrow, lamin expression is reduced to enable nuclear deformation and facilitate the migration of cells through small pores. However, in megakaryocytes that do not exit the bone marrow, lamin expression is increased to augment the rigidity of the nucleus (Shin *et al.,* 2013). In addition to the mechanical properties of lamins, changes in chromatin organization are also correlated with lamin expression during B-cell maturation. During the transition between naïve B cells and memory B cells, LmnB1 is transiently downregulated to release chromatin from the NE and enable somatic hypermutations (Klymenko *et al.,* 2018). These studies exemplify the functional importance of lamins and how their expression is purposefully regulated in specific cell types.

Lamin misregulation in cancer

Lamins have long been implicated in cancer given their function in regulating nuclear shape and size, two basic criteria for cytological diagnosis of cancer. Tumor biopsies show increased nuclear size and irregularities in both nuclear contour and chromatin organization in comparison to non-tumor tissues (Chow *et al.,* 2012). This suggests a role for lamins in tumorigenesis, and recently it has been shown that lamins are aberrantly expressed in various tumors, and in some cases, associated with higher tumor grade and poor prognosis. (Willis *et al.,* 2008; Jia *et al.,* 2019).

Although LmnA and LmnB1 are found to be both up and downregulated in cancer, an interesting observation is the overexpression (OE) of LmnB1 that is observed in many different tumor tissues (Li *et al.,* 2013; Radspieler *et al.,* 2019; Gu *et al.,* 2020; Yi *et al.,* 2020; Li *et al.,* 2020). LmnB1 OE is also associated with higher tumor grade and poor prognosis in certain

cancer types, suggesting a role for LmnB1 in tumorigenesis (Sun *et al.,* 2010; Gu *et al.,* 2020). The mechanistic effects of LmnB1 OE in the context of cancer have not been well studied, but two recent papers suggest that LmnB1 OE may sequester and inhibit proteins important for telomere protection and the DNA damage response (Pennarun *et al.,* 2021; Etourneaud *et al.,* 2021). This may lead to telomere dysfunction, persistent DNA damage, and genetic instability, which may all be contributing factors in disease progression. Given that LmnB1 has many other reported functions, such as roles in chromatin organization and gene expression, it will be interesting to determine how these processes may also be affected by LmnB1 OE.

References

Aebi, U., Cohn, J., Buhle, L., & Gerace, L. The nuclear lamina is a meshwork of intermediate-type filaments. *Nature*. **323**, 560-564 (1986).

Beck, M., & Hurt, E. The nuclear pore complex: understanding its function through structural insight. *Nat. Rev. Mol. Cell Biol.* **18**, 73-89 (2017).

Belgareh, N., Rabut, G., Bai, S.W., van Overbeek, M., Beaudouin, J., Daigle, N., Zatsepina, O.V., Pasteau, F., Labas, V., Fromont-Racine, M., Ellenberg, J., & Doye, V. An evolutionarily conserved NPC subcomplex, which redistributes in part to kinetochores in mammalian cells. *J. Cell Biol.* **154**, 1147-1160 (2001).

Blobel, G. Gene gating: A hypothesis. *Proc. Nati. Acad. Sci. USA.* **82**, 8527-8529 (1985).

Capell, B.C., & Collins, F.S. Human laminopathies: nuclei gone genetically awry. *Nat. Rev. Genet.* **7**, 940-952 (2006).

Capelson, M., Liang, Y., Schulte, R., Mair, W., Wagner, U., & Hetzer, M.W. Chromatin-bound nuclear pore components regulate gene expression in higher eukaryotes. *Cell.* **140**, 372–383 (2010).

Capitanio, J.S., Montpetit, B., & Wozniak, R.W. Human Nup98 regulates the localization and activity of DExH/D-box helicase DHX9. *Elife*. **6**, e18825 (2017).

Chakraborty, P., Wang, Y., Wei, J.H., van Deursen, J., Yu, H., Malureanu, L., Dasso, M., Forbes, D.J., Levy, D.E., Seemann, J., & Fontoura, B.M. Nucleoporin levels regulate cell cycle progression and phase-specific gene expression. *Dev. Cell*. **15**, 657–667 (2008).

De Vos, W.H., Houben, F., Kamps, M., Malhas, A., Verheyen, F., Cox, J., Manders, E.M., Verstraeten, V.L., van Steensel, M.A., Marcelis, C.L., van den Wijngaard, A., Vaux, D.J., Ramaekers, F.C., & Broers, J.L. Repetitive disruptions of the nuclear envelope invoke temporary loss of cellular compartmentalization in laminopathies. *Hum. Mol. Genet.* **20**, 4175-4186 (2011).

Denais, C.M., Gilbert, R.M., Isermann, P., McGregor, A.L., te Lindert, M., Weigelin, B., Davidson, P.M., Friedl, P., Wolf, K., & Lammerding, J. Nuclear envelope rupture and repair during cancer cell migration. *Science*. **352**, 353-358 (2016).

Earle, A.J., Kirby, T.J., Fedorchak, G.R., Isermann, P., Patel, J., Iruvanti, S., Moore, S.A., Bonne, G., Wallrath, L.L., & Lammerding, J. Mutant lamins cause nuclear envelope rupture and DNA damage in skeletal muscle cells. *Nat. Mater*. **19**, 464-473 (2020).

Etourneaud, L., Moussa, A., Rass, E., Genet, D., Willaume, S., Chabance-Okumura, C., Wanschoor, P., Picotto, J., Thézé, B., Dépagne, J., Veaute, X., Dizet, E., Busso, D., Barascu, A., Irbah, L., Kortulewski, T., Campalans, A., Le Chalony, C., Zinn-Justin, S.,

Scully, R., Pennarun, G., Bertrand, P. Lamin B1 sequesters 53BP1 to control its recruitment to DNA damage. *Sci Adv.* **7**, eabb3799 (2021).

Franks, T.M., McCloskey, A., Shokirev, M.N., Benner, C., Rathore, A. & Hetzer, M.W. Nup98 recruits the Wdr82-Set1A/COMPASS complex to promoters to regulate H3K4 trimethylation in hematopoietic progenitor cells. *Genes Dev.* **31**,1–13 (2017).

Goss, V. L., Hocevar, B. A., Thompson, L. J., Stratton, C. A., Burns, D. J., & Fields, A. P. Identification of nuclear beta II protein kinase C as a mitotic lamin kinase. *J Biol Chem.* **269**, 19074–19080 (1994).

Gu, Y., Li, J., Guo, D., Chen, B., Liu, P., Xiao, Y., Yang, K., Liu, Z., & Liu, Q. Identification of 13 Key Genes Correlated With Progression and Prognosis in Hepatocellular Carcinoma by Weighted Gene Co-expression Network Analysis. *Front Genet.* **11**, 153 (2020).

Harel, A., Orjalo, A.V., Vincent, T., Lachish-Zalait, A., Vasu, S., Shah, S., Zimmerman, E., Elbaum, M., & Forbes, D.J. Removal of a single pore subcomplex results in vertebrate nuclei devoid of nuclear pores. *Mol. Cell*. **11**, 853-864 (2003).

Ibarra, A., Benner, C., Tyagi, S., Cool, J., & Hetzer, M.W. Nucleoporin-mediated regulation of cell identity genes. *Genes Dev.* **30**, 2253-2258 (2016).

Ivorra, C., Kubicek, M., González, J. M., Sanz-González, S. M., Alvarez-Barrientos, A., O'Connor, J. E., Burke, B., & Andrés, V. A mechanism of AP-1 suppression through interaction of c-Fos with lamin A/C. *Genes Dev.* **20**, 307–320 (2006).

Jacinto, F.V., Brenner, C., & Hetzer, M.W. The nucleoporin Nup153 regulates embryonic stem cell pluripotency through gene silencing. *Genes Dev.* **29**,1224–1238 (2015).

Jia, Y., Vong, J. S., Asafova, A., Garvalov, B. K., Caputo, L., Cordero, J., Singh, A., Boettger, T., Günther, S., Fink, L., Acker, T., Barreto, G., Seeger, W., Braun, T., Savai, R., & Dobreva, G. Lamin B1 loss promotes lung cancer development and metastasis by epigenetic derepression of RET. *J Exp Med.* **216**, 1377–1395 (2019).

Kalverda, B., Pickersgill, H., Shloma, V.V., & Fornerod, M. Nucleoporins directly stimulate expression of developmental and cell-cycle genes inside the nucleoplasm. *Cell*. **140**, 360–371 (2010).

Kindermann, B., Valkova, C., Kramer, A., Perner, B., Engelmann, C., Behrendt, L., Kritsch, D., Jungnickel, B., Kehlenbach, R.H., Oswald, F., Englert, C., & Kaether, C. The nuclear pore proteins Nup88/214 and T-cell acute lymphatic leukemia-associated NUP214 fusion proteins regulate Notch signaling. *J. Biol. Chem.* **294**, 11741–11750 (2019).

Klymenko, T., Bloehdorn, J., Bahlo, J., Robrecht, S., Akylzhanova, G., Cox, K., Estenfelder, S., Wang, J., Edelmann, J., Strefford, J. C., Wojdacz, T. K., Fischer, K., Hallek, M., Stilgenbauer, S., Cragg, M., Gribben, J., & Braun, A. Lamin B1 regulates somatic

mutations and progression of B-cell malignancies. *Leukemia*. **32**, 364–375 (2018).

Li, L., Du, Y., Kong, X., Li, Z., Jia, Z., Cui, J., Gao, J., Wang, G., & Xie, K. Lamin B1 is a novel therapeutic target of betulinic acid in pancreatic cancer. *Clin Cancer Res*. **19**, 4651–4661 (2013).

Li, W., Li, X., Li, X., Li, M., Yang, P., Wang, X., Li, L., & Yang, B. Lamin B1 Overexpresses in Lung Adenocarcinoma and Promotes Proliferation in Lung Cancer Cells via AKT Pathway. *Onco Targets Ther.* **13**, 3129–3139 (2020).

Liang, Y., Franks, T.M., Marchetto, M.C., Gage, F.H., & Hetzer, M.W. Dynamic association of NUP98 with the human genome. *PLoS Genet.* **9**, e1003308 (2013).

McKeon, F. D., Kirschner, M. W., & Caput, D. Homologies in both primary and secondary structure between nuclear envelope and intermediate filament proteins. *Nature*. **319**, 463–468 (1986).

Moir, R. D., Yoon, M., Khuon, S., & Goldman, R. D. Nuclear lamins A and B1: different pathways of assembly during nuclear envelope formation in living cells. *J Cell Biol.* **151**, 1155–1168 (2000).

Paddy, M. R., Belmont, A. S., Saumweber, H., Agard, D. A., & Sedat, J. W. Interphase nuclear envelope lamins form a discontinuous network that interacts with only a fraction of the chromatin in the nuclear periphery. *Cell*. **62**, 89–106 (1990).

Panda, D., Pascual-Garcia, P., Dunagin, M., Tudor, M., Hopkins, K.C., Xu, J., Gold, B., Raj, A., Capelson, M., & Cherry, S. Nup98 promotes antiviral gene expression to restrict RNA viral infection in Drosophila. *Proc. Natl. Acad. Sci. USA*. **111**, E3890–E3899 (2014).

Pascual-Garcia, P., Jeong, J., & Capelson, M. Nucleoporin Nup98 associates with Trx/MLL and NSL histone-modifying complexes and regulates Hox gene expression. *Cell Rep.* **9**, 433–442 (2014).

Pascual-Garcia, P., Debo, B., Aleman, J.R., Talamas, J.A., Lan, Y., Nguyen, N.H., Won, K.J., & Capelson, M. Metazoan nuclear pores provide a scaffold for poised genes and mediate induced enhancer-promoter contacts. *Mol. Cell*. **66**, 63-76 (2017).

Pennarun, G., Picotto, J., Etourneaud, L., Redavid, A. R., Certain, A., Gauthier, L. R., Fontanilla-Ramirez, P., Busso, D., Chabance-Okumura, C., Thézé, B., Boussin, F. D., & Bertrand, P. Increase in lamin B1 promotes telomere instability by disrupting the shelterin complex in human cells. *Nucleic Acids Res*. **49**, 9886–9905 (2021).

Peter, M., Nakagawa, J., Dorée, M., Labbé, J. C., & Nigg, E. A. In vitro disassembly of the nuclear lamina and M phase-specific phosphorylation of lamins by cdc2 kinase. *Cell*. **61**, 591–602 (1990).

Pott, S., & Lieb, J.D. What are super-enhancers? *Nat. Genet.* **47**, 8-12 (2015).

Prestel, M., Feller, C., Straub, T., Mitlohner, H., & Becker, P.B. The activation potential of MOF is constrained for dosage compensation. *Mol. Cell*. **38**, 815–826 (2010).

Rabut, G., Doye, V., & Ellenberg, J. Mapping the dynamic organization of the nuclear pore complex inside single living cells. *Nat. Cell Biol*. **6**, 1114-1121 (2004).

Radspieler, M. M., Schindeldecker, M., Stenzel, P., Försch, S., Tagscherer, K. E., Herpel, E., Hohenfellner, M., Hatiboglu, G., Roth, W., & Macher-Goeppinger, S. Lamin-B1 is a senescence-associated biomarker in clear-cell renal cell carcinoma. *Oncol Lett.* **18**, 2654–2660 (2019).

Raja, S.J., Charapitsa, I., Conrad, T., Vaquerizas, J.M., Gebhardt, P., Holz, H., Kadlec, J., Fraterman, S., Luscombe, N.M., & Akhtar, A. The nonspecific lethal complex is a transcriptional regulator in Drosophila. *Mol. Cell*. **38**, 827–841 (2010).

Rupaimoole, R., & Slack, F. J. MicroRNA therapeutics: towards a new era for the management of cancer and other diseases. *Nat. Rev Drug Discov*. **16**, 203–222 (2017).

Shimi, T., Pfleghaar, K., Kojima, S., Pack, C. G., Solovei, I., Goldman, A. E., Adam, S. A., Shumaker, D. K., Kinjo, M., Cremer, T., & Goldman, R. D. The A- and B-type nuclear lamin networks: microdomains involved in chromatin organization and transcription. *Genes Dev.* **22**, 3409–3421 (2008).

Shimi, T., Kittisopikul, M., Tran, J., Goldman, A. E., Adam, S. A., Zheng, Y., Jaqaman, K., & Goldman, R. D. Structural organization of nuclear lamins A, C, B1, and B2 revealed by superresolution microscopy. *Mol. Biol. Cell.* **26**, 4075–4086 (2015).

Shin, J. W., Spinler, K. R., Swift, J., Chasis, J. A., Mohandas, N., & Discher, D. E. Lamins regulate cell trafficking and lineage maturation of adult human hematopoietic cells. *Proc. Natl. Acad. Sci. USA.* **110**, 18892–18897 (2013).

Singer, S., Zhao, R., Barsotti, A.M., Ouwehand, A., Fazollahi, M., Coutavas, E., Breuhahn, K., Neumann, O., Longerich, T., Pusterla, T., Powers, M.A., Giles, K.M., Leedman, P.J., Hess, J., Grunwald, D., Bussemaker, H.J., Singer, R.H., Schirmacher, P., & Prives, C. Nuclear pore component Nup98 is a potential tumor suppressor and regulates posttranscriptional expression of select p53 target genes. *Mol. Cell.* **48**, 799–810 (2012).

Stick, R., Angres, B., Lehner, C. F., & Nigg, E. A. The fates of chicken nuclear lamin proteins during mitosis: evidence for a reversible redistribution of lamin B2 between inner nuclear membrane and elements of the endoplasmic reticulum. *J Cell Biol.* **107**, 397–406 (1988).

Sullivan, T., Escalante-Alcalde, D., Bhatt, H., Anver, M., Bhat, N., Nagashima, K., Stewart, C. L., & Burke, B. Loss of A-type lamin expression compromises nuclear envelope integrity leading to muscular dystrophy. *J Cell Biol.* **147**, 913–920 (1999).

Sun, S., Xu, M. Z., Poon, R. T., Day, P. J., & Luk, J. M. Circulating Lamin B1 (LMNB1) biomarker detects early stages of liver cancer in patients. *J Proteome Res.* **9**, 70–78 (2010).

Thompson, L. J., Bollen, M., & Fields, A. P. Identification of protein phosphatase 1 as a mitotic lamin phosphatase. *J Biol. Chem.* **272**, 29693–29697 (1997).

Toyama, B.H., Savas, J.N., Park, S.K., Harris, M.S., Ingolia, N.T., Yates, J.R., & Hetzer, M.W. Identification of long-lived proteins reveals exceptional stability of essential cellular structures. *Cell*. **154**, 971-982 (2013).

Ullman, K.S., Shah, S., Powers, M.A., & Forbes, D.J. The nucleoporin nup153 plays a critical role in multiple types of nuclear export. *Mol. Biol. Cell*. **10**, 649–664 (1999).

van Deursen, J., Boer, J., Kasper, L., & Grosveld, G. G2 arrest and impaired nucleocytoplasmic transport inmouse embryoslackingtheproto-oncogene CAN/Nup214. *EMBO J.* **15**, 5574-5583 (1996).

Van de Vosse, D.W., Wan, Y., Lapetina, D.L., Chen, W., Chiang, J., Aitchison, J.D., & Wozniak, R.W. A role for the nucleoporin Nup170p in chromatin structure and gene silencing. *Cell*. **152**, 969–983 (2013).

Vargas, J. D., Hatch, E. M., Anderson, D. J., & Hetzer, M. W. Transient nuclear envelope rupturing during interphase in human cancer cells. *Nucleus*. **3**, 88–100 (2012).

Vergnes, L., Péterfy, M., Bergo, M. O., Young, S. G., & Reue, K. Lamin B1 is required for mouse development and nuclear integrity. *Proc. Nati. Acad. Sci. USA*. **101**, 10428–10433 (2004).

Willis, N. D., Cox, T. R., Rahman-Casañs, S. F., Smits, K., Przyborski, S. A., van den Brandt, P., van Engeland, M., Weijenberg, M., Wilson, R. G., de Bruïne, A., & Hutchison, C. J. Lamin A/C is a risk biomarker in colorectal cancer. *PloS One.* **3**, e2988 (2008).

Wong, J. J., Ritchie, W., Ebner, O. A., Selbach, M., Wong, J. W., Huang, Y., Gao, D., Pinello, N., Gonzalez, M., Baidya, K., Thoeng, A., Khoo, T. L., Bailey, C. G., Holst, J., & Rasko, J. E. Orchestrated intron retention regulates normal granulocyte differentiation. *Cell*. **154**, 583–595 (2013).

Wu, X., Kasper, L.H., Mantcheva, R.T., Mantchev, G.T., Springett, M.J., & van Deursen, J.M.A. Disruption of the FG nucleoporin NUP98 causes selective changes in nuclear pore complex stoichiometry and function. *Proc. Natl. Acad. Sci. USA*. **98**, 3191-3196 (2001).

Yi, M., Li, T., Qin, S., Yu, S., Chu, Q., Li, A., & Wu, K. Identifying Tumorigenesis and Prognosis-Related Genes of Lung Adenocarcinoma: Based on Weighted Gene Coexpression Network Analysis. *Biomed Res Int.* **2020**, 4169691 (2020).

Chapter 2: Nup98/96 knockdown disrupts the nuclear lamina through Lamin B1

Introduction

NPCs and the nuclear lamina are physically linked at the NE, and depend on each other for proper assembly and organization (Al-Haboubi *et al.,* 2011; Xie *et al.,* 2016; Hawryluk-Gara *et al.,* 2005; Smythe *et al.,* 2000). Lamins require NPCs for their import into the nucleus, while NPCs depend on lamins for their anchoring and distribution across the NE (Newport *et al.,* 1990; Chaudhary and Courvalin, 1993; Moir *et al.,* 2000; Lenz-Bohme *et al.,* 1997; Liu *et al.,* 2000; Xie *et al.,* 2016). Some studies have extended this interdependence between NPCs and the nuclear lamina beyond organization to functionality of the complexes. Mutations or deletions of lamin proteins alter NPC positioning and composition, as well as Nup localization and stability, and ultimately disrupt protein import through NPCs (Busch *et al.,* 2009; Giacomini *et al.,* 2015; Lussi *et al.,* 2000). Conversely, Nup deletions alter nuclear morphology and lamin organization, but no consequences to lamin function have been reported (Wente and Blobel, 1993; Siniossoglou *et al.,* 1996; Hawryluk-Gara *et al.,* 2005; Zhou and Pante, 2010). We uncovered a potential link between two specific Nups, Nup98 and Nup96 (Nup98/96), in regulating the function of the nuclear lamina, by demonstrating that small interfering RNA (siRNA) mediated knockdown (KD) of Nup98/96 impairs nuclear integrity.

Nup98/96 are two of ~30 distinct Nups that comprise the NPC. These are the only Nups that are encoded by the same mRNA transcript (Nup98/96 mRNA), translated together as an ~186 kDa protein, and undergo autoproteolysis to yield two separate Nups (Rosenblum and Blobel, 1999; Fontoura *et al.,* 1999). Nup98 is a peripheral Nup that functions in association with the NPC and also independently within the nucleoplasm. At NPCs, Nup98 facilitates the transport of mRNAs across the NE through the interaction between mRNAs, mRNA export factors, and the FG repeats on Nup98 (Radu *et al.,* 1995; Pritchard *et al.,* 1999; Blevins *et al.,*

2003). Within the nucleoplasm, Nup98 regulates gene expression at the transcriptional and post-transcriptional level, as described in Chapter 1 (Capelson *et al.,* 2010; Pasqual-Garcia *et al.,* 2014; Franks *et al.,* 2017; Capitanio *et al.,* 2017; Singer *et al.,* 2012).

Nup96 is a scaffold Nup that is essential in NPC assembly during interphase and at the end of mitosis. This Nup is recruited early during NPC assembly as part of the Nup107-160 complex, and its recruitment is required for proper assembly of the remaining Nups (Doucet *et al.,* 2010). Nup96 is also suggested to function in mRNA export of select genes, such as those involved in the immune response and cell cycle (Faria *et al.,* 2006; Chakraborty *et al.,* 2008). Evidently, Nup98/96 have broad functions in NPC assembly, nucleocytoplasmic transport, and gene regulation, and we wanted to determine how these Nups might regulate the nuclear lamina.

Results

Nup98/96 knockdown disrupts lamin assembly

Immunofluorescence imaging revealed that KD of Nup98/96, using siRNA oligonucleotides targeting the Nup96 portion of the Nup98/96 transcript, significantly disrupts the nuclear lamina (Figure 2.1). This disruption is characterized by an enlarged lamina meshwork across the nuclear surface, and can be quantified by calculating the percentage of the nuclear surface area lacking LmnA fluorescence (Figure 2.2a). Applying this analysis in both U2OS and RPE1 cells, Nup98/96 KD significantly disrupts the nuclear lamina (Figure 2.2b).

Transfection with an alternative siRNA oligonucleotide targeting the Nup98 portion of the Nup98/96 transcript similarly perturbed the lamina meshwork (Figure 2.3a). However, this phenotype was not observed upon KD of other scaffold Nups required for NPC assembly, such as Nup107 (Figure 2.3a). Further, KD of Nup98/96 did not impair LmnA protein import or bulk mRNA export (Figure 2.3b; Figure 2.4). Taken together, this suggests that the lamin phenotype observed upon Nup98/96 KD is independent from NPC assembly and transport, and Nup98/96 may have a novel role in regulating the nuclear lamina.

Nup98/96 knockdown disrupts nuclear integrity

Since disruptions to the nuclear lamina have been previously shown to increase the frequency of transient NE rupture, we assessed whether Nup98/96 KD also displayed a similar phenotype. Using a previously developed reporter cell line (U2OS GFP-NLS; Vargas *et al.,* 2012), cells were treated with the indicated siRNA for 48 hours, followed by live cell imaging every 3 minutes over a 24 hour period to monitor nuclear integrity. Temporary mislocalization of the GFP-NLS signal into the cytoplasm and its relocalization back into the nucleus was

indicative of the nuclear rupture and repair event (Figure 2.5a). Nup98/96 KD significantly increased the frequency of transient NE rupture to over 40% of cells, compared to less than 3% of cells in both the Luciferase KD and Nup107 KD conditions, suggesting that the disruption to the nuclear lamina caused by Nup98/96 KD impacts nuclear integrity (Figure 2.5b).

siRNA resistant Nup98/96 expression rescues the lamin phenotype upon knockdown of Nup98/96

The disruption to the lamina network upon KD of Nup98/96 can be restored by expressing an exogenous full-length siRNA resistant Nup98/96 construct, as assessed using the nuclear surface area analysis described above (Figure 2.6). However, expression of either exogenous Nup98 or Nup96 alone only partially rescued the lamin phenotype, suggesting that both Nup98 and Nup96, or its full length transcript, is required for proper lamin assembly.

Nup98/96 knockdown disrupts the nuclear lamina through LmnB1 expression

To understand how Nup98/96 KD perturbs the nuclear lamina, we assessed the mRNA and protein expression of the major A-type and B-type lamin isoforms: LmnA, LmnB1, and LmnB2. Nup98/96 KD specifically reduced LmnB1 mRNA and protein expression, while LmnA and LmnB2 expression remained unchanged (Figure 2.7).

We then hypothesized that the increased frequency of transient NE rupture we observed previously was a consequence of reduced LmnB1 expression. To test this, we overexpressed either mCherry or mCherry-LmnB1 in the U2OS GFP-NLS reporter cell line, and monitored nuclear integrity 48 hours after Nup98/96 siRNA transfection. Expression of mCherry-LmnB1 reduced the frequency of transient NE rupture to less than 10% of cells, compared to a rupture

frequency of ~30% of cells that express mCherry alone (Figure 2.8). This suggests a link between Nup98/96 KD and regulation of nuclear integrity through LmnB1 expression.

Discussion

Here we suggest a novel function for two specific Nups, Nup98/96, in regulating the nuclear lamina. Although Nup98/96, and more broadly NPCs, are implicated in nucleocytoplasmic transport, impaired bulk mRNA export or lamin protein import did not cause the changes to the lamin network upon Nup98/96 KD. Rather, Nup98/96 siRNA treatment modulated the expression of LmnB1, which is the lamin isoform responsible for seeding assembly of the nuclear lamina (Shimi *et al.,* 2008). LmnB1 depletion alone resulted in a similar disruption to the lamina, further supporting our data linking Nup98/96 KD with defects in lamin assembly, through LmnB1 expression.

The lamin disruption observed upon KD of Nup98/96 was associated with a weakened lamina that was more susceptible to transient NE rupture. Multiple non-lethal rupture and repair events occurred in individual nuclei, which was similar to the increased rupture frequency observed when lamins are depleted or mutated (De Vos *et al.,* 2011; Vargas *et al.,* 2012). We further show that the increased rupture frequency upon Nup98/96 KD is a consequence of reduced LmnB1 expression. Altogether this suggests a novel function of Nup98/96 in regulating LmnB1 expression for proper lamin assembly and nuclear integrity.

This link between Nup98/96 and LmnB1 is not only important in understanding the organizational and functional interdependence between NPCs and the nuclear lamina, but also has interesting applications in the context of diseases that harbor mutations or altered expression of Nup98/96. The most notable example is acute myeloid leukemia (AML), in which a subset of patients harbor chromosomal translocations involving the N-terminus of Nup98 fused to the C-terminus of one of 30 different proteins. Although Nup98 translocations in AML are quite rare,

they are associated with poor prognosis, and are more prevalent in pediatric cases (~6-10%) in comparison to adult cases (~1-2%) (Xu *et al.,* 2016).

Many studies have characterized the transcriptional defects caused by these Nup98 fusion proteins as an explanation for the development of leukemia (Franks *et al.*, 2017: Xu *et al.,* 2016). However, if Nup98/96 also regulates LmnB1 expression and the functionality of the nuclear lamina, this may be an additional factor that may disrupt cellular homeostasis. Given that LmnB1 has essential roles in chromatin organization and maintenance of nuclear integrity, altered LmnB1 expression may promote aberrant transcriptional programs and accumulation of DNA damage (van Steensel and Belmont, 2017; Chen *et al.,* 2020). It will therefore be important to investigate the regulatory link between Nup98/96 and LmnB1 by probing the mechanism involved in misregulating LmnB1 expression.

Based on our rescue experiment, in which Nup98 or Nup96 expression could not fully prevent lamin disruption upon KD of Nup98/96, this suggested that both proteins are required to regulate LmnB1 expression. Given that Nup98 and Nup96 have been characterized to function in transcriptional and post-transcriptional gene regulation, these proteins may directly affect the transcription, splicing, or stability of LmnB1. However, since RNAs are also reported to post-transcriptionally regulate gene expression, it is possible that the Nup98/96 mRNA itself may have a novel function in regulating LmnB1 expression (Poliseno *et al.,* 2010; Tay *et al.,* 2011). It will therefore be important to determine if LmnB1 undergoes transcriptional or post-transcriptional regulation upon Nup98/96 KD, in order to uncover the mechanism and novel functions of Nup98/96 proteins or the mRNA transcript in regulating LmnB1 expression.

Materials and Methods

Cell culture and transfection

U2OS cells were cultured in DMEM supplemented with 10% fetal bovine serum and 1% penicillin-streptomycin. RPE1 cells were cultured in DMEM/F12 with 10% fetal bovine serum, 1% penicillin-streptomycin, and 0.01 mg/mL hygromycin B. Plasmids were transfected with Lipofectamine 2000 (Thermo Fisher Scientific) and siRNAs were transfected with siLentFect (Bio-Rad), both according to the manufacture's instructions.

Plasmids and siRNA sequences

The plasmids and siRNA oligonucleotides used in this chapter are listed in Table 2.1 and Table 2.2, respectively. Gateway cloning was used to generate the pQCXIB plasmids, and In-Fusion cloning was used to generate the pLVXTP plasmids. The pLVXTP backbone was linearized using Not1 and EcoR1 restriction sites, and was provided by Rusty Gage's lab.

The VSV-M sequence was cloned from the pEGFPN3-M-GFP plasmid (von Kobbe *et al.,* 2000), provided by Beatriz Fontoura's lab. The UTRs of Nup98/96 (NM_016320) were cloned from cDNA prepared using SuperScript II Reverse Transcriptase (Invitrogen) and oligo(dT) primers. The same 5' and 3' UTRs were added to the FLAG-Nup98/96, FLAG-Nup98, and FLAG-Nup96 plasmids.

The Nup96 sequence within the FLAG-Nup98/96 and FLAG-Nup96 plasmids was designed to be siRNA resistant by changing 5 bases within the siRNA binding site (NM016320.5: Nucleotides 3919-3937). These underlined nucleotide changes (5'- GCACAGATCGTTAAACATT-3') did not alter the amino acid sequence, and were introduced into the Nup96 sequence with the primers used for PCR.

Stable cell lines

Stable cell lines used in this chapter are listed in Table 2.3. These were made by transfecting the indicated plasmids into the parental cell line, and selecting with the appropriate antibiotic for 2 weeks. Fluorescence activated cell sorting was used to select GFP and mCherry positive cells in the U2OS GFP-NLS mCherry-LmnB1 cell line.

Immunofluorescence imaging and analysis

Cells were grown on coverslips and fixed with 4% PFA in 1x PBS for 5 minutes at room temperature. Coverslips were blocked with IF buffer (10 mg/mL BSA, 0.1% Triton-X-100, 0.02% SDS, diluted in 1x PBS) for 20 minutes prior to incubation with primary and secondary antibodies diluted in IF buffer. The primary antibodies used are listed in Table 2.4. Coverslips were briefly incubated with Hoechst (1 ug/mL, Molecular Probes) and mounted in ProLong Gold (Thermo Fisher Scientific). Imaging was performed on a Zeiss LSM710 scanning confocal microscope and Leica SP8 confocal microscope with a 63x 1.4NA oil immersion objective.

Fiji was used to analyze fluorescence intensity and the lamin disruption across the nuclear surface. Nuclear fluorescence intensity was quantified for LmnA and mAb414, and the values were normalized to the average fluorescence intensity observed in untreated cells. The lamin disruption was quantified by calculating the percentage of the nuclear surface area lacking LmnA fluorescence for each individual cell per condition. Z slices of the nuclear surface were thresholded prior to analysis.

Fluorescent in situ hybridization (FISH) imaging and analysis

Cells were grown on poly-lysine coated coverslips and prepared according to the Stellaris RNA-FISH protocol. 5' FAM labeled PolyT(25)Vn LNA detection probes (Qiagen) were used at a final concentration of 250 nM. Imaging was performed on a Leica SP8 confocal microscope with a 63x 1.4NA oil immersion objective.

Fiji, along with the Extended Depth of Field and Morphology plugins, was used to segment the nucleus and cytoplasm of each cell and measure the fluorescence intensity of the 5' FAM polyT probe. The background fluorescence intensity for each image was subtracted from the described measurements and the cytoplasmic to nuclear ratio of fluorescence intensity for each cell in each knockdown or overexpression condition was calculated. Only the mCherry positive cells were selected for analysis in the overexpression condition. R and RStudio were used for statistical analysis of the data.

Live cell imaging

Cells expressinf 3xGFP-NLS were plated in 8-well μ-slide chambers (iBidi) and imaged on a Zeiss Axioscope/Yokogawa spinning disk confocal microscope 48 hours after siRNA transfection. Cells were monitored for 18-24 hours, with images taken every 3 minutes. The percentage of rupturing cells was determined manually for >300 nuclei per condition. A nucleus that underwent at least one non-lethal rupture and repair event was counted as a rupturing cell.

Real-time PCR (qPCR)

RNA was prepared using the RNeasy kit (Qiagen) and cDNA was prepared using the Quantitect Reverse Transcription kit (Qiagen), both according to the manufacture's instructions.

qPCR was performed on a BIO-RAD CFX384 Real-Time System using the resulting cDNA, SYBR Green PCR Master Mix (Thermo Fisher Scientific), and qPCR primers listed in Table 2.5. ΔΔCt analysis with normalization to Rpl4 was used to calculate relative gene expression.

Western blotting

Cells were lysed in RIPA buffer (50 mM Tris-HCl pH 8, 150 mM NaCl, 1% Triton-X, 0.5% sodium deoxycholate, and 0.1% SDS) and protein concentration was normalized using the BCA protein assay (Thermo Fisher Scientific). Membranes were blocked using 5% nonfat milk in 1x TBST for 15 min prior to incubation with primary and secondary antibodies diluted in blocking buffer. The primary antibodies used are listed in Table 2.4. Secondary antibodies were conjugated to fluorescent dyes or HRP for detection.

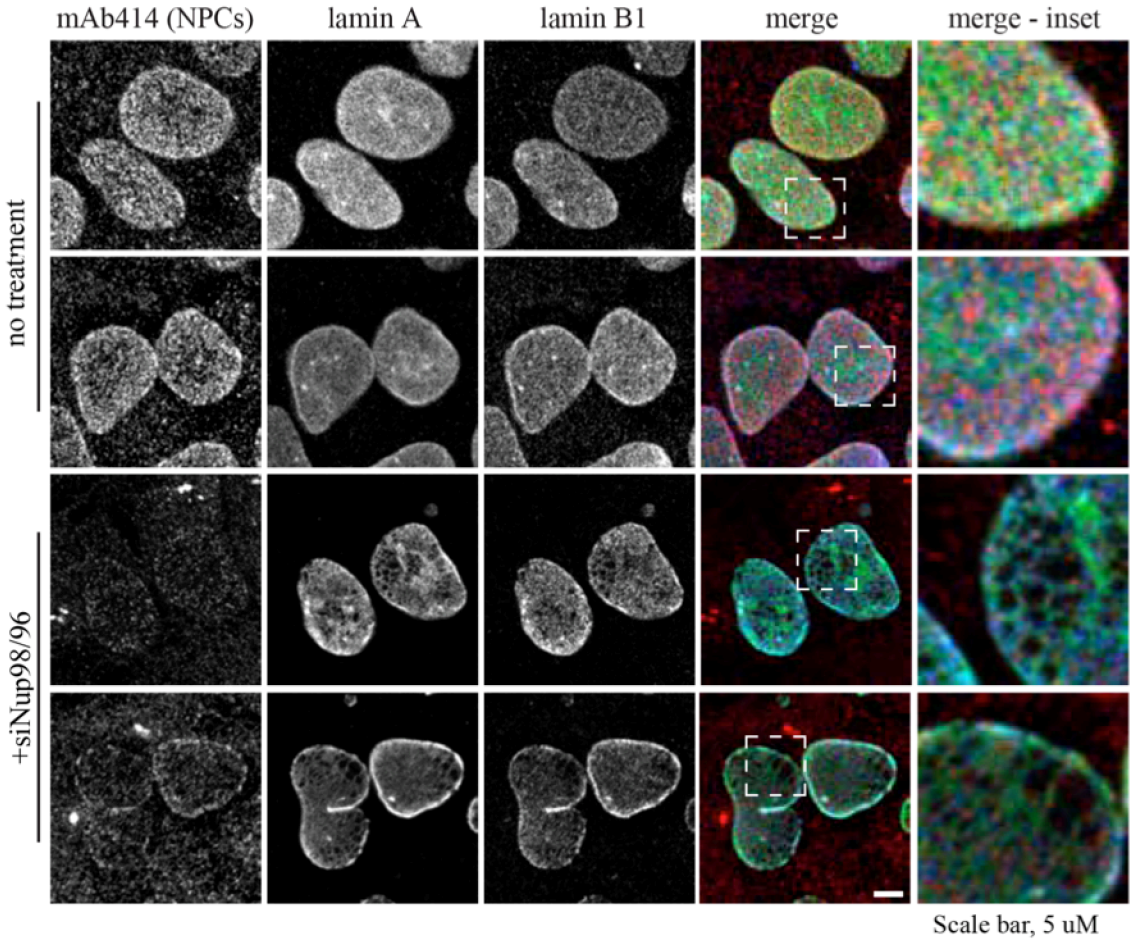

Figure 2.1. Nup98/96 knockdown disrupts the nuclear lamina
U2OS cells were untreated or treated with Nup98/96 siRNA for 72 hours and labeled with antibodies recognizing NPCs (mAb414), LmnA, and LmnB1 for immunofluorescence imaging. Confocal images of the nuclear surface are shown.

a.

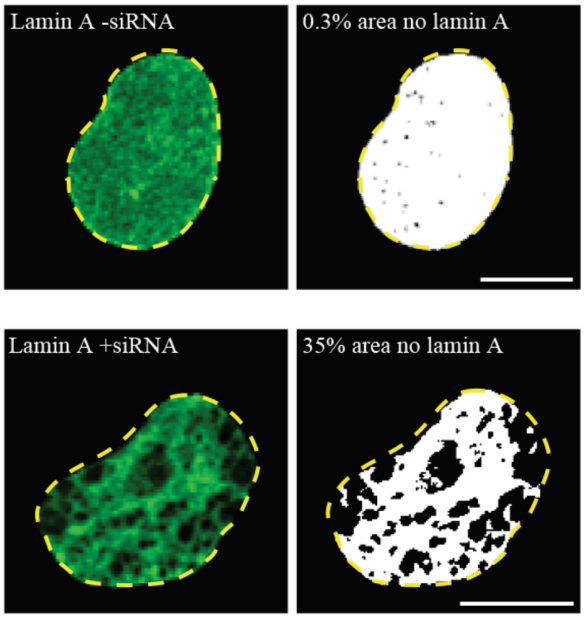

b.

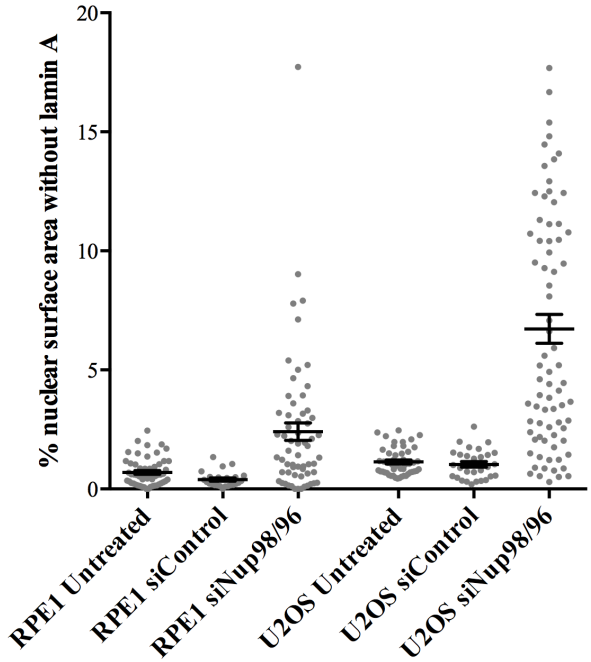

Figure 2.2. Nup98/96 knockdown increases the percentage of the nuclear surface area lacking LmnA

a. Representative fluorescence (left) and thresholded (right) images of the nuclear surface of U2OS cells labeled with LmnA used to quantify the percentage of lamin free regions on the nuclear surface in untreated cells (top) and cells transfected with Nup98/96 siRNA (bottom) for 72 hours. Scale bar is 10 μm. b. U2OS and RPE1 cells were treated with the indicated siRNA for 72 hours and labeled with LmnA for immunofluorescence based analysis of the percentage of lamin free regions across the nuclear surface. Error bars were computed as standard error of the mean over three biological replicates.

a.

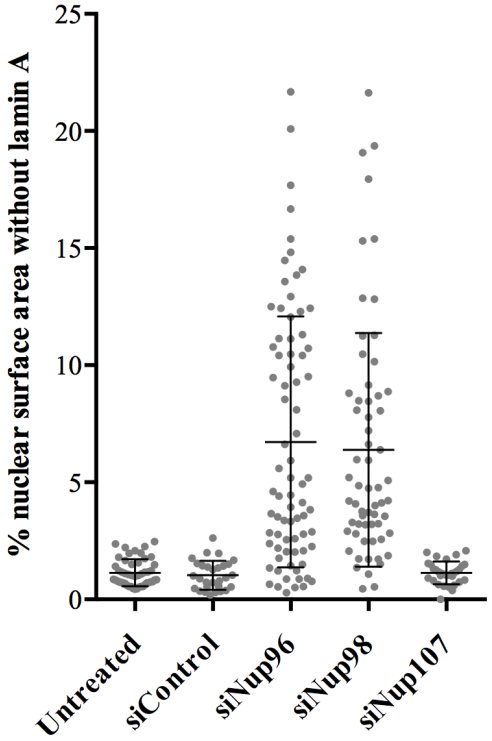

b.

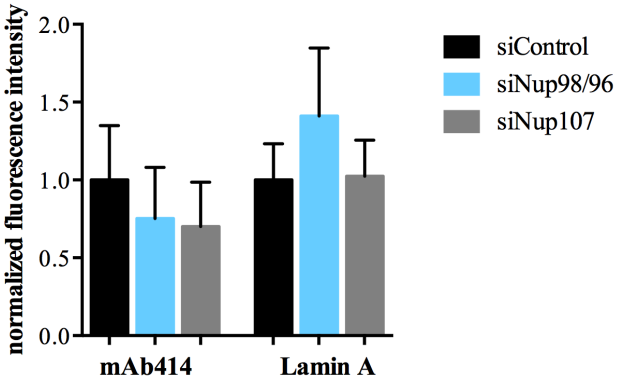

Figure 2.3. Disruptions to the nuclear lamina are specific to Nup98/96 knockdown, and are not a consequence of impaired LmnA import

a. U2OS cells were treated with the indicated siRNA for 72 hours and labeled with LmnA for immunofluorescence based analysis of the percentage of lamin free regions across the nuclear surface. Over 100 nuclei were analyzed per condition. Error bars were computed as standard deviation over three biological replicates. b. U2OS cells were treated with the indicated siRNA for 72 hours and the normalized fluorescence intensity of mAb414 (NPCs) and LmnA was quantified and plotted relative to untreated cells for each KD condition. Error bars were computed as standard deviation over three biological replicates.

a.

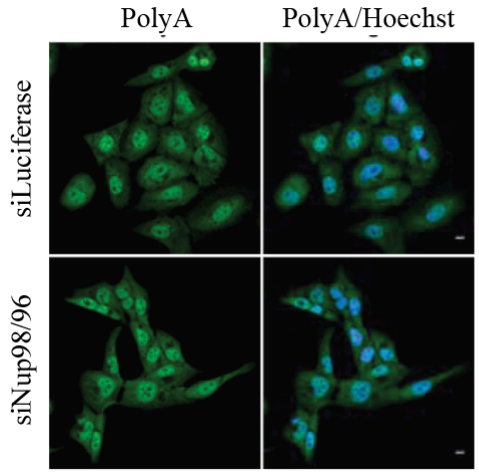

b.

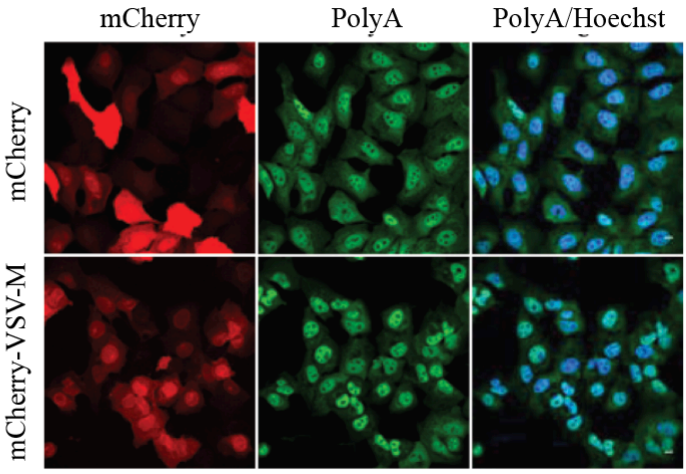

c.

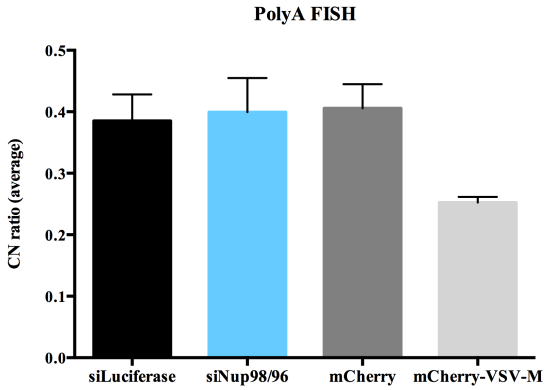

Figure 2.4. Nup98/96 knockdown does not affect the cytoplasmic to nuclear ratio of bulk mRNA

a. U2OS cells were treated with the indicated siRNA for 48 hours and hybridized with PolyA probes. b. U2OS cells were transfected with mCherry or mCherry-VSV-M for 24 hours and hybridized with PolyA probes. Confocal images of a single z-slice are shown. Scale bar is 10 μm. c. Cytoplasmic to nuclear (CN) ratios of bulk mRNA signal visualized with PolyA probes were computed for U2OS cells treated with the indicated siRNA for 48 hours, or expressing the indicated plasmid for 24 hours. Only mCherry positive cells were selected for CN analysis.

a.

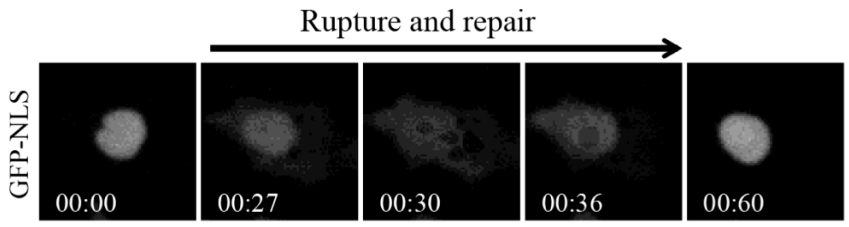

b.

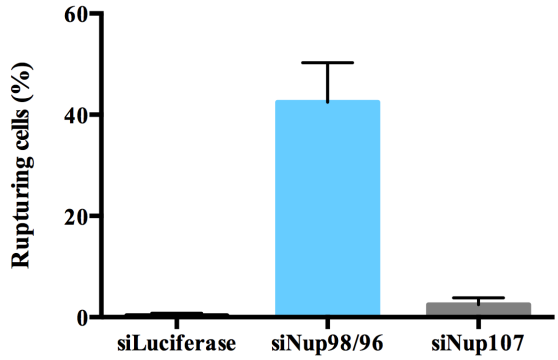

Figure 2.5. Nup98/96 knockdown increases the frequency of transient nuclear envelope rupture

a. Representative fluorescence images depicting the nuclear envelope rupture and repair event in U2OS cells expressing 3xGFP-NLS and treated with Nup98/96 siRNA for 48 hours. Time in hours: minutes. b. U2OS cells expressing 3xGFP-NLS were treated with the indicated siRNA for 48 hours and subsequently imaged every 3 minutes for 24 hours. ~400 nuclei per condition were monitored to calculate the percentage of cells undergoing transient nuclear envelope rupture. Nuclei that ruptured at least once during the timecourse were counted as a rupturing cell. Error bars were computed as standard deviation over three biological replicates.

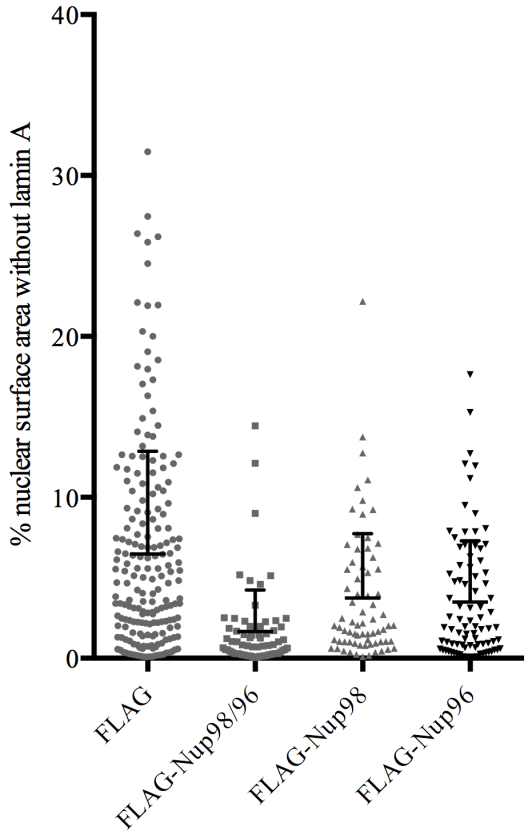

Figure 2.6. siRNA resistant Nup98/96 rescues the lamin disruption upon Nup98/96 knockdown

U2OS cells expressing FLAG, FLAG-Nup98/96 (siRNA resistant), FLAG-Nup98, or FLAG-96 (siRNA resistant) were treated with Nup96 specific siRNA oligonucleotides and labeled with LmnA to calculate the percentage of lamin free regions across the nuclear surface. FLAG expression was induced 6 hours prior to siRNA transfection, and cells were collected after 72 hours of siRNA knockdown. Error bars were computed as standard deviation over three biological replicates.

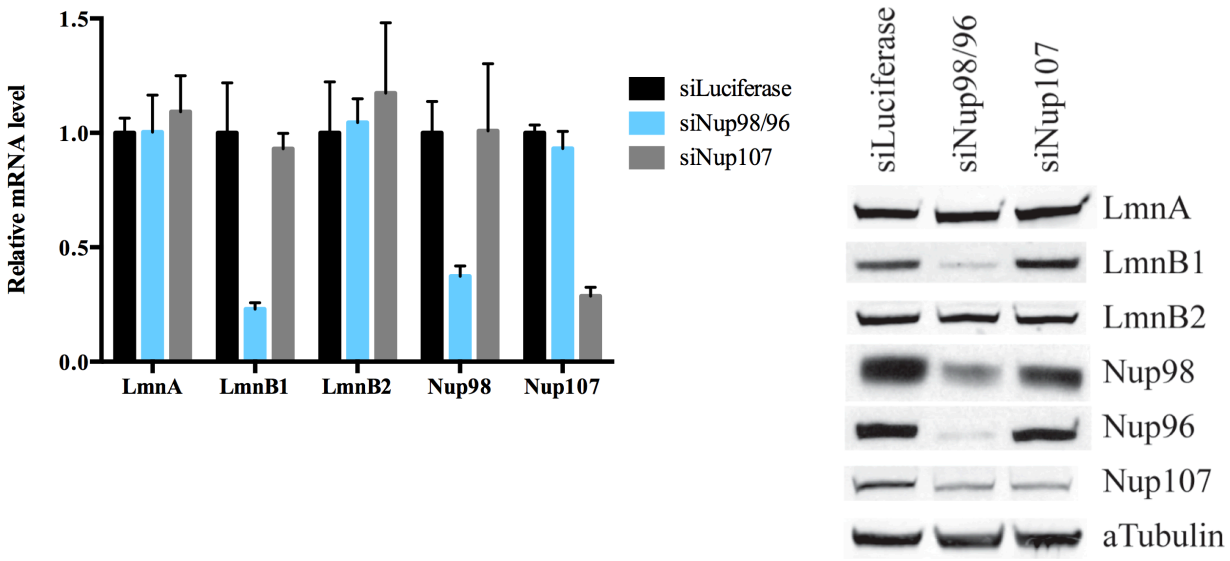

Figure 2.7. Nup98/96 knockdown specifically affects LmnB1 mRNA and protein expression
U2OS cells were treated with the indicated siRNA for 48 hours and mRNA expression of three lamin isoforms (LmnA, LmnB1, LmnB2) were analyzed by qPCR and western blot. Relative mRNA levels normalized to RPL4 are plotted. Error bars were computed as standard deviation over three biological replicates.

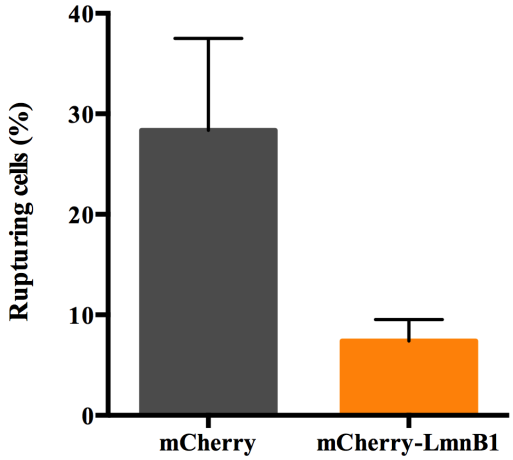

Figure 2.8. Exogenous LmnB1 expression reduces the frequency of transient nuclear envelope rupture after knockdown of Nup98/96
U2OS cells expressing 3xGFP-NLS and either mCherry or mCherry-LmnB1 were treated with Nup98/96 siRNA for 48 hours and subsequently imaged every 3 minutes for 24 hours. ~300 nuclei per condition were monitored to calculate the percentage of cells undergoing transient nuclear envelope rupture. Nuclei that ruptured at least once during the timecourse were counted as a rupturing cell. Error bars were computed as standard deviation over three biological replicates.

Table 2.1. List of plasmids – Chapters 2 and 3

Plasmid name	Constitutive or inducible expression
pQCXIB mCherry	Constitutive
pQCXIB mCherry-LmnB1	Constitutive
pQCXIB mCherry-VSV-M	Constitutive
pLVXTP FLAG	Inducible (Doxycyline, 2 ug/mL)
pLVXTP FLAG-Nup98/96 (aa 1-1817)	Inducible (Doxycyline, 2 ug/mL)
pLVXTP FLAG-Nup98 (aa 1-920)	Inducible (Doxycyline, 2 ug/mL)
pLVXTP FLAG-Nup96 (aa 881-1817)	Inducible (Doxycyline, 2 ug/mL)
pQCXIB miniSOG-LmnB1	Constitutive
pQCXIB miniSOG-LmnB1-3UTR	Constitutive

Table 2.2. List of siRNA sequences – Chapters 2 and 3

siRNA name	Sense sequence (5' – 3')	Final concentration
siLuciferase[1]	UAUGCAGUUGCUCUCCAGCdTdT	20 nM
siNup98	GAGAGAGAUUUAGUUUCCUAAGCAAdTdT	25 nM
siNup96[2*]	GCACAAAUUGUGAAGCACUdTdT	50 nM
siNup107[2]	CUGCGAAUACACUUUCUUCdTdT	50 nM
siNup98-2	CACAAAUACCAGUGGGAAUdTdT	50 nM
siNup96-2	GAAGAAGCAUUUCAGAAUAdTdT	50 nM

[1]siRNA sequence from Ibarra *et al.,* 2016. [2]siRNA sequence from Doucet *et al.,* 2010.
*Also referred to as siNup98/96 throughout the dissertation.

Table 2.3. List of stable cell lines – Chapters 2 and 3

Parental cell line (plasmid)	Transfection or Infection (Selection)
U2OS (GFP-NLS)[1]	Transfection (G418)
U2OS GFP-NLS (pQCXIB mCherry)	Transfection (G418; Blasticidin)
U2OS GFP-NLS (pQCXIB mCherry-LmnB1)	Transfection (G418; Blasticidin)
U2OS (pLVXTP FLAG)	Transfection (Puromycin)
U2OS (pLVXTP FLAG-Nup98/96)	Transfection (Puromycin)
U2OS (pLVXTP FLAG-Nup98)	Transfection (Puromycin)
U2OS (pLVXTP FLAG-Nup96)	Transfection (Puromycin)
RPE1 (pQCXIB miniSOG-LmnB1)	Infection (Blasticidin)
RPE1 (pQCXIB miniSOG-LmnB1-3UTR)	Infection (Blasticidin)

[1]Reporter cell line from Vargas *et al.,* 2012.

Table 2.4. List of antibodies – Chapters 2 and 3

Antibody	Company	Dilution for IF	Dilution for WB
LmnA	Sigma-Aldrich, L1293	1:1000	1:1000
LmnB1	Santa Cruz Biotechnology, sc-6216	1:1000	1:1000
LmnB2	Abcam, ab8983		1:1000
mAb414	Covance, mms-120R	1:1000	
Nup98	Cell Signaling, #2292		1:1000
Nup96	Abcam, ab124980		1:1000
aTubulin	Sigma, T5168		1:5000
Flag	Sigma, F1804	1:1000	

Table 2.5. List of qPCR primers – Chapters 2 and 3

qPCR primers	Sequence (5' – 3')
Rpl4	Forward: GCCCTTCGAGCACCACGCA
	Reverse: TGGCTTGTAGTGCCGCTGCTG
LmnA	Forward: GGTGGTGACGATCTGGGCT
	Reverse: CCAGTGGAGTTGATGAGAGC
LmnB1	Forward: AAGGCGAAGAAGAGAGGTTGAAG
	Reverse: GCGGAATGAGAGATGCTAACACT
LmnB1-Intron7	Forward: AGCGGAAGAGGGTTGATGTG
	Reverse: GCAATCCACAAAGCCTTGCTA
LmnB1-Intron10	Forward: ATTTTTCCTTCTGTTTTCCTCATCA
	Reverse: CTGAGAAGGCTCTGCACTGT
LmnB2	Forward: ATCAAGGCGCTGTACGAGTC
	Reverse: TCTTGGCGCTCTTGTTGACC
miniSOG	Forward: AAATTCTGGAACCTCCTGCAC
	Reverse: TGCACTCCGATGAAATACTGGA
Nup98	Forward: CTGTTGGTTCGACCCTGTTT
	Reverse: CCAAGAGCTGTTCCAAATCC
Nup96	Forward: ACTTGTGGGAAGTGCTGAGG
	Reverse: CACGTATGCCTGAGTTGTCA
Nup107	Forward: CTGCTTCCGGGTCGAAGGGC
	Reverse: AAAGCCACTCCTGTCCATGGCT

Acknowledgements

We thank Abigail Buchwalter for immunofluorescence characterization of the lamin disruption phenotype and development of the nuclear surface area analysis; Juliana S. Capitanio for help with the cytoplasmic to nuclear ratio of bulk mRNA analysis; the Salk Flow Cytometry core for assistance sorting the U2OS GFP-NLS mCherry-LmnB1 cell line for GFP and mCherry positive cells; and the Salk Waitt Advanced Biophotonics core for access to the Zeiss spinning disk confocal microscope for live cell imaging.

Chapter 2 is unpublished material coauthored with Buchwalter, Abigail and Capitanio, Juliana S. The dissertation author, under guidance of Martin W. Hetzer, was the primary researcher and author of this material.

References

Al-Haboubi, T., Shumaker, D. K., Köser, J., Wehnert, M., & Fahrenkrog, B. Distinct association of the nuclear pore protein Nup153 with A- and B-type lamins. *Nucleus.* **2**, 500–509 (2011).

Blevins, M. B., Smith, A. M., Phillips, E. M., & Powers, M. A. Complex formation among the RNA export proteins Nup98, Rae1/Gle2, and TAP. *J Biol. Chem.* **278**, 20979–20988 (2003).

Busch, A., Kiel, T., Heupel, W. M., Wehnert, M., & Hübner, S. Nuclear protein import is reduced in cells expressing nuclear envelopathy-causing lamin A mutants. *Exp. Cell Res.* **315**, 2373–2385 (2009).

Capelson, M., Liang, Y., Schulte, R., Mair, W., Wagner, U., & Hetzer, M.W. Chromatin-bound nuclear pore components regulate gene expression in higher eukaryotes. *Cell.* **140**, 372–383 (2010).

Capitanio, J.S., Montpetit, B., & Wozniak, R.W. Human Nup98 regulates the localization and activity of DExH/D-box helicase DHX9. *Elife*. **6**, e18825 (2017).

Chakraborty, P., Wang, Y., Wei, J.H., van Deursen, J., Yu, H., Malureanu, L., Dasso, M., Forbes, D.J., Levy, D.E., Seemann, J., & Fontoura, B.M. Nucleoporin levels regulate cell cycle progression and phase-specific gene expression. *Dev. Cell*. **15**, 657–667 (2008).

Chaudhary, N., & Courvalin, J. C. Stepwise reassembly of the nuclear envelope at the end of mitosis. *J Cell Biol.* **122**, 295–306 (1993).

Chen, N. Y., Kim, P. H., Fong, L. G., & Young, S. G. Nuclear membrane ruptures, cell death, and tissue damage in the setting of nuclear lamin deficiencies. *Nucleus.* **11**, 237–249 (2020).

De Vos, W.H., Houben, F., Kamps, M., Malhas, A., Verheyen, F., Cox, J., Manders, E.M., Verstraeten, V.L., van Steensel, M.A., Marcelis, C.L., van den Wijngaard, A., Vaux, D.J., Ramaekers, F.C., & Broers, J.L. Repetitive disruptions of the nuclear envelope invoke temporary loss of cellular compartmentalization in laminopathies. *Hum. Mol. Genet.* **20**, 4175-4186 (2011).

Doucet, C. M., Talamas, J. A., & Hetzer, M. W. Cell cycle-dependent differences in nuclear pore complex assembly in metazoa. *Cell*. **141**, 1030–1041 (2010).

Faria, A. M., Levay, A., Wang, Y., Kamphorst, A. O., Rosa, M. L., Nussenzveig, D. R., Balkan, W., Chook, Y. M., Levy, D. E., & Fontoura, B. M. The nucleoporin Nup96 is required for proper expression of interferon-regulated proteins and functions. *Immunity*. **24**, 295–304 (2006).

Fontoura, B. M., Blobel, G., & Matunis, M. J. A conserved biogenesis pathway for nucleoporins: proteolytic processing of a 186-kilodalton precursor generates Nup98 and the novel nucleoporin, Nup96. *J Cell Biol.* **144**, 1097–1112 (1999).

Franks, T.M., McCloskey, A., Shokirev, M.N., Benner, C., Rathore, A. & Hetzer, M.W. Nup98 recruits the Wdr82-Set1A/COMPASS complex to promoters to regulate H3K4 trimethylation in hematopoietic progenitor cells. *Genes Dev.* **31**,1–13 (2017).

Giacomini, C., Mahajani, S., Ruffilli, R., Marotta, R., & Gasparini, L. Lamin B1 protein is required for dendrite development in primary mouse cortical neurons. *Mol. Biol.* Cell. **27**, 35–47 (2016).

Hawryluk-Gara, L. A., Shibuya, E. K., & Wozniak, R. W. Vertebrate Nup53 interacts with the nuclear lamina and is required for the assembly of a Nup93-containing complex. *Mol. Biol. Cell.* **16**, 2382–2394 (2005).

Ibarra, A., Benner, C., Tyagi, S., Cool, J., & Hetzer, M.W. Nucleoporin-mediated regulation of cell identity genes. *Genes Dev.* **30**, 2253-2258 (2016).

Lenz-Böhme, B., Wismar, J., Fuchs, S., Reifegerste, R., Buchner, E., Betz, H., & Schmitt, B. Insertional mutation of the Drosophila nuclear lamin Dm0 gene results in defective nuclear envelopes, clustering of nuclear pore complexes, and accumulation of annulate lamellae. *J Cell Biol.* **137**, 1001–1016 (1997).

Liu, J., Rolef Ben-Shahar, T., Riemer, D., Treinin, M., Spann, P., Weber, K., Fire, A., & Gruenbaum, Y. Essential roles for Caenorhabditis elegans lamin gene in nuclear organization, cell cycle progression, and spatial organization of nuclear pore complexes. *Mol. Biol. Cell.* **11**, 3937–3947 (2000).

Lussi, Y. C., Hügi, I., Laurell, E., Kutay, U., & Fahrenkrog, B. The nucleoporin Nup88 is interacting with nuclear lamin A. *Mol. Biol. Cell.* **22**, 1080–1090 (2011).

Moir, R. D., Yoon, M., Khuon, S., & Goldman, R. D. Nuclear lamins A and B1: different pathways of assembly during nuclear envelope formation in living cells. *J Cell Biol.* **151**, 1155–1168 (2000).

Newport, J. W., Wilson, K. L., & Dunphy, W. G. A lamin-independent pathway for nuclear envelope assembly. *J Cell Biol.* **111**, 2247–2259 (1990).

Pascual-Garcia, P., Jeong, J., & Capelson, M. Nucleoporin Nup98 associates with Trx/MLL and NSL histone-modifying complexes and regulates Hox gene expression. *Cell Rep.* **9**, 433–442 (2014).

Poliseno, L., Salmena, L., Zhang, J., Carver, B., Haveman, W. J., & Pandolfi, P. P. A coding-independent function of gene and pseudogene mRNAs regulates tumour biology. *Nature*. **465**, 1033–1038 (2010).

Pritchard, C. E., Fornerod, M., Kasper, L. H., & van Deursen, J. M. RAE1 is a shuttling mRNA export factor that binds to a GLEBS-like NUP98 motif at the nuclear pore complex through multiple domains. *J Cell Biol.* **145**, 237–254 (1999).

Radu, A., Moore, M. S., & Blobel, G. The peptide repeat domain of nucleoporin Nup98 functions as a docking site in transport across the nuclear pore complex. *Cell*. **81**, 215–222 (1995).

Rosenblum, J. S., & Blobel, G. Autoproteolysis in nucleoporin biogenesis. *Proc. Nati. Acad. Sci. USA*. **96**, 11370–11375 (1999).

Shimi, T., Pfleghaar, K., Kojima, S., Pack, C. G., Solovei, I., Goldman, A. E., Adam, S. A., Shumaker, D. K., Kinjo, M., Cremer, T., & Goldman, R. D. The A- and B-type nuclear lamin networks: microdomains involved in chromatin organization and transcription. *Genes Dev.* **22**, 3409–3421 (2008).

Singer, S., Zhao, R., Barsotti, A.M., Ouwehand, A., Fazollahi, M., Coutavas, E., Breuhahn, K., Neumann, O., Longerich, T., Pusterla, T., Powers, M.A., Giles, K.M., Leedman, P.J., Hess, J., Grunwald, D., Bussemaker, H.J., Singer, R.H., Schirmacher, P., & Prives, C. Nuclear pore component Nup98 is a potential tumor suppressor and regulates posttranscriptional expression of select p53 target genes. *Mol. Cell.* **48**, 799–810 (2012).

Siniossoglou, S., Wimmer, C., Rieger, M., Doye, V., Tekotte, H., Weise, C., Emig, S., Segref, A., & Hurt, E. C. A novel complex of nucleoporins, which includes Sec13p and a Sec13p homolog, is essential for normal nuclear pores. *Cell.* **84**, 265–275 (1996).

Smythe, C., Jenkins, H. E., & Hutchison, C. J. Incorporation of the nuclear pore basket protein nup153 into nuclear pore structures is dependent upon lamina assembly: evidence from cell-free extracts of Xenopus eggs. *EMBO J.* **19**, 3918–3931 (2000).

Tay, Y., Kats, L., Salmena, L., Weiss, D., Tan, S. M., Ala, U., Karreth, F., Poliseno, L., Provero, P., Di Cunto, F., Lieberman, J., Rigoutsos, I., & Pandolfi, P. P. Coding-independent regulation of the tumor suppressor PTEN by competing endogenous mRNAs. *Cell*. **147**, 344–357 (2011).

van Steensel, B., & Belmont, A. S. Lamina-Associated Domains: Links with Chromosome Architecture, Heterochromatin, and Gene Repression. *Cell.* **169**, 780–791 (2017).

Vargas, J. D., Hatch, E. M., Anderson, D. J., & Hetzer, M. W. Transient nuclear envelope rupturing during interphase in human cancer cells. *Nucleus*. **3**, 88–100 (2012).

von Kobbe C, van Deursen JM, Rodrigues, J. P., Sitterlin, D., Bachi, A., Wu, X., Wilm, M., Carmo-Fonseca, M., & Izaurralde, E. Vesicular stomatitis virus matrix protein inhibits host cell gene expression by targeting the nucleoporin Nup98. *Mol. Cell.* **6**, 1243–1252 (2000).

Wente, S. R., & Blobel, G. A temperature-sensitive NUP116 null mutant forms a nuclear envelope seal over the yeast nuclear pore complex thereby blocking nucleocytoplasmic traffic. *J Cell Biol.* **123**, 275–284 (1993).

Xie, W., Chojnowski, A., Boudier, T., Lim, J. S., Ahmed, S., Ser, Z., Stewart, C., & Burke, B. A-type Lamins Form Distinct Filamentous Networks with Differential Nuclear Pore Complex Associations. *Curr. Biol.* **26**, 2651–2658 (2016).

Xu, H., Valerio, D. G., Eisold, M. E., Sinha, A., Koche, R. P., Hu, W., Chen, C. W., Chu, S. H., Brien, G. L., Park, C. Y., Hsieh, J. J., Ernst, P., & Armstrong, S. A. NUP98 Fusion Proteins Interact with the NSL and MLL1 Complexes to Drive Leukemogenesis. *Cancer Cell.* **30**, 863–878 (2016).

Zhou, L., & Panté, N. The nucleoporin Nup153 maintains nuclear envelope architecture and is required for cell migration in tumor cells. *FEBS Lett.* **584**, 3013–3020 (2010).

Chapter 3: Nup98/96 siRNA oligonucleotides post-transcriptionally regulate Lamin B1

Introduction

Nup98 and Nup96 function in gene regulation, as described in Chapters 1 and 2, suggesting that these proteins might transcriptionally or post-transcriptionally regulate LmnB1 expression. However, it is also possible that the Nup98/96 mRNA transcript has a novel function in regulating LmnB1 expression. This is based on the competing endogenous RNA (ceRNA) hypothesis, which postulates that mRNA transcripts can post-transcriptionally regulate the expression of other mRNA transcripts by competing for microRNAs (miRNAs) (Seitz, 2009; Salmena *et al.,* 2011).

miRNAs are ~22 nucleotide long small noncoding RNAs that post-transcriptionally regulate gene expression. These miRNAs associate with Argonaute (Ago) proteins to form a miRNA-induced silencing complex (miRISC). Nucleotides 2-8 at the 5' end of the miRNA form the seed region that directs the miRISC to miRNA response elements (MREs) encoded within mRNA transcripts, and the nucleotides at the 3' end provide further specificity and stabilization of the miRNA:mRNA interaction. miRISC then recruits effector proteins, such that miRISC binding within the 5' UTR or coding sequence of mRNA transcripts inhibits translation, while binding within the 3' UTR promotes mRNA decay (Filipowicz *et al.,* 2008; Hausser *et al.,* 2013; Lytle *et al.,* 2007)

Since the proposition of the ceRNA hypothesis, several studies have identified specific mRNAs, pseudogenes, and long noncoding RNAs that function as ceRNAs (Poliseno *et al.,* 2010; Tay *et al.,* 2010; Li *et al.,* 2016). Additionally, several miRNAs have already been shown to target LmnB1, suggesting that this may be a plausible mechanism through which Nup98/96 regulates LmnB1 expression (Lin and Fu, 2009; Setijono et al., 2018). Therefore, we aimed to

determine if Nup98/96 post-transcriptionally regulates LmnB1 expression, and whether this is mediated through miRNAs.

Results

Nup98/96 knockdown post-transcriptionally regulates LmnB1 expression

To understand how Nup98/96 regulates LmnB1 mRNA, we utilized real-time PCR (qPCR) to determine whether LmnB1 is being misregulated transcriptionally or post-transcriptionally. We observed that Nup98/96 siRNA treatment reduced the expression of mature, spliced LmnB1 mRNA, as detected by qPCR primers spanning an exon-exon junction. However, there was no effect on the LmnB1 pre-mRNA transcript, using two different intron-spanning qPCR primers, suggesting regulation after transcription and splicing (Figure 3.1a). We further confirmed that Nup98/96 post-transcriptionally regulates LmnB1 mRNA by demonstrating that an exogenous LmnB1 construct can be similarly downregulated upon siRNA KD of Nup98/96, and that its regulation is dependent on the LmnB1 3' UTR (Figure 3.1b).

Nup98/96 knockdown destabilizes LmnB1 mRNA

Given that LmnB1 is being downregulated through its 3' UTR upon Nup98/96 KD, this suggested that the stability of LmnB1 mRNA may be altered. To address this, we inhibited transcription using Actinomycin D (ActD), and used mRNA sequencing to monitor the decay of LmnB1 mRNA 48 hours after Nup98/96 siRNA transfection. This showed a destabilization of LmnB1 mRNA with a >60% reduction in its half-life when compared to the luciferase KD condition in two biological replicates (Figure 3.2).

We also assessed global mRNA dynamics and identified nine other mRNA transcripts that may be similarly affected by Nup98/96 siRNA transfection (Table 3.1). These mRNA targets were identified through two important filters. First, the expression of the transcript must be at least 50% downregulated at 48 hours post siRNA transfection, specifically in the Nup98/96

KD condition. Second, the mRNA half life must be calculated in all three KD conditions (luciferase, Nup98/96, and Nup107) and decreased by at least 40% in the Nup98/96 KD compared to the luciferase KD, and also by at least 20% in the Nup98/96 KD compared to the Nup107 KD. This analysis identified 10 mRNA transcripts, including LmnB1, that are destabilized in both biological replicates upon Nup98/96 KD, and are listed in descending order based on their change in stability compared to the luciferase siRNA control (Table 3.1).

LmnB1 mRNA is regulated by miRNAs

As we began to probe the mechanism through which Nup98/96 might regulate LmnB1 mRNA stability, we made an interesting observation that implicated the Nup98/96 mRNA in this process. LmnB1 mRNA expression was significantly reduced 6 hours post siRNA transfection, a time point where Nup98/96 mRNA expression is decreased, but Nup98 and Nup96 protein expression is unchanged (Figure 3.3). This was observed in both U2OS cells and RPE1 cells (data not shown), suggesting a novel function for the Nup98/96 mRNA transcript.

To understand how Nup98/96 mRNA might regulate RNA stability, we first identified all of the RNA transcripts that are post-transcriptionally regulated at 6 hours post Nup98/96 siRNA transfection using total RNA-sequencing. This technique allowed us to separate transcriptional and post-transcriptional targets based on their intronic and exonic reads, and we identified 69 post-transcriptional targets regulated by Nup98/96 mRNA (Figure 3.4; Table 3.2).

Based on the ceRNA hypothesis and the fact that lamins are post-transcriptionally regulated by miRNAs, we asked whether the 69 post-transcriptional targets shared a common miRNA binding site. We found enrichment for a GAAGCACA motif in the 3' UTRs of these 69

transcripts, and the top two miRNAs suggested to target this motif are hsa-miR-218 and hsa-miR-636 (Figure 3.5).

We confirmed that hsa-miR-218 and hsa-miR-636 regulate LmnB1 expression by transfecting cells with miRNA mimics and demonstrating that LmnB1 mRNA expression is decreased (Figure 3.6). To determine if these miRNAs are involved in Nup98/96 mediated regulation of LmnB1 expression, we used miRNA inhibitors to test if LmnB1 mRNA can be protected upon KD of Nup98/96. Inhibition of hsa-miR-218 and hsa-miR-636 showed a partial rescue of LmnB1 mRNA expression in the absence of Nup98/96, but was only significant for the hsa-miR-636 inhibitor (Figure 3.7-3.8).

To understand how Nup98/96 mRNA might regulate hsa-miR-636, we asked whether Nup98/96 mRNA could bind and sequester hsa-miR-636 away from its targets. We analyzed the association between Nup98/96 mRNA and a 3' biotin tagged hsa-miR-636 mimic (hsa-miR-636-bio) through biotin immunoprecipitation and qPCR. hsa-miR-636-bio showed increased fold binding for LmnB1 mRNA, but not Nup98/96 mRNA in the average of two biological replicates (Figure 3.9). This confirmed LmnB1 as a novel target of hsa-miR-636, but suggested that exogenous hsa-miR-636 mimics do not interact with Nup98/96 mRNA.

We then asked whether hsa-miR-636 preferentially loaded into the RISC upon KD of Nup98/96 using an Argonaute 2 immunoprecipitation followed by TaqMan miRNA qPCR. However, we did not see any enrichment for hsa-miR-636 at 4 hours post siRNA treatment, a time point at which LmnB1 mRNA expression is already reduced by 50% (Figure 3.10). Further, there was no enrichment for hsa-miR-636 at 20 hours post siRNA treatment (data not shown).

Nup98/96 siRNA oligonucleotides can mimic miRNAs that regulate LmnB1

Finally, we noticed sequence similarities between the siRNA oligonucleotides targeting Nup98/96 and miRNAs hsa-miR-218 and hsa-miR-636 (Table 3.3). The similarities were within the seed regions of the miRNAs and anti-sense siRNAs, which are nucleotides 2-8 starting at the 5' end of the oligonucleotide. In the case of miRNAs, this seed region determines which mRNA transcripts are targeted for degradation or translational repression, and LmnB1 is predicted to have a binding site for these miRNAs within its 3' UTR. This suggested that the siRNA oligonucleotides used to KD Nup98/96 might have off target effects on LmnB1 by mimicking hsa-miR-218 and hsa-miR-636. To test this idea, we designed two new siRNA oligonucleotides (siNup98-2, siNup96-2) to target Nup98/96 that did not contain the same seed sequence as these miRNAs (Table 2.2). These siRNAs properly knocked down Nup98/96 mRNA and protein expression, but had no effect on LmnB1 mRNA or protein expression (Figure 3.11). This supported our hypothesis that LmnB1 is an off target effect of the original siRNAs used against Nup98/96, based on the presence of a miRNA binding site for hsa-miR-218 and hsa-miR-636 within its 3' UTR.

Discussion

Here we show that LmnB1 is post-transcriptionally regulated through its 3' UTR upon Nup98/96 KD, and is one of the top genes with reduced half life estimates. We further demonstrate that the regulation of LmnB1 mRNA expression occurs within 6 hours post siRNA transfection, suggesting that the Nup98/96 mRNA may function as a ceRNA to regulate LmnB1 expression. Given that the ceRNA hypothesis is based on competition for miRNAs, we searched for common miRNA motifs within the 3' UTRs of the transcripts post-transcriptionally regulated at 6 hours post siRNA transfection, and identified an enrichment for hsa-miR-218 and hsa-miR-636 binding sites. We confirmed that hsa-miR-218 and hsa-miR-636 regulate LmnB1 expression and validated LmnB1 as a novel target of hsa-miR-636. However, we were not able to determine the mechanism through which Nup98/96 mRNA might regulate hsa-miR-636.

Rather, we uncovered an off target effect on LmnB1 from the siRNA oligonucleotides used against Nup98/96 in our studies. siRNAs have been reported to have off target effects by mimicking miRNAs through their seed regions, and the two siRNA oligonucleotides used to KD Nup98/96 have almost identical seed sequences with the miRNAs for hsa-miR-218 and hsa-miR-636 (Lin *et al.,* 2005; Jackson *et al.,* 2006). We confirmed that the regulation of LmnB1 was an off target effect by designing two additional siRNAs against Nup98/96 that differed in the seed region and demonstrating that these properly knocked down Nup98/96, but had no effect on LmnB1 mRNA or protein expression.

Based on these results, there appears to be no regulatory link between Nup98/96 and the nuclear lamina, through LmnB1. Rather, the organizational and functional defects of the nuclear lamina that we observed upon KD of Nup98/96 are a result of an siRNA off target effect on LmnB1 expression.

Materials and Methods

Cell culture and transfection

U2OS cells were cultured in DMEM supplemented with 10% fetal bovine serum and 1% penicillin-streptomycin. RPE1 cells were cultured in DMEM/F12 with 10% fetal bovine serum, 1% penicillin-streptomycin, and 0.01 mg/mL hygromycin B. siRNAs and miRNA mimics/inhibitors were transfected with siLentFect (Bio-Rad), according to the manufacture's instructions.

Plasmids and siRNA sequences

The plasmids and siRNA oligonucleotides used in this chapter are listed in Table 2.1 and Table 2.2. Gateway cloning was used to generate the pQCXIB plasmids. The 3' UTR of LmnB1 (NM_005573) was cloned from cDNA prepared using SuperScript II Reverse Transcriptase (Invitrogen) and Oligo(dT) primers.

Stable cell lines

Stable cell lines used in this chapter are listed in Table 2.3. These were made using retroviral infection of the transfer plasmid and selection with the appropriate antibiotic for 2 weeks. Retroviral packaging was completed in 293T cells, transfected with the ampho packaging plasmid and the transfer plasmid using polyethylenimine. The media was changed 16 hours after transfection, and collected 48 hours after transfection. This viral media was passed through a 0.45 μm filter, and added directly to the cell line of interest with 6 ug/mL polybrene.

Actinomycin D mRNA-sequencing and mRNA half life estimation

Cells were seeded in 6-well plates and transfected with siRNA for 48 hours. Actinomycin D (ActD) was added at a final concentration of 5 ug/mL, and cells were collected at 0, 2, 3, and 4 hours post ActD treatment. RNA was isolated using Trizol (Ambion) and purified with the RNeasy kit (Qiagen). RNA from *Saccharomyces cerevisiae* was added to comprise 10% of the total RNA used for library preparation with the TruSeq stranded mRNA kit (Illumina). Libraries were run on the Illumina HiSeq system (single end 50).

After quality check and trimming, sequencing data was aligned to human reference sequence GRCh38 (hg38) and annotated with the corresponding gencode GTF file using the genome aligner STAR. The number of exonic reads per gene was calculated using featureCounts (from Rsubread package). After filtering out low expression genes, differential expression was assessed using DESeq2 at 48 hours post siRNA transfection (0 hours ActD), and the genes whose expression was specifically decreased by 50% only in the Nup98/96 KD condition were selected for downstream analysis. The spike-in normalized read counts for these misregulated genes were plotted over the ActD timecourse. The rate of mRNA decay was calculated as $ln(normalized\ mRNA\ counts) = intercept + k_{decay} * time$, then filtered for line-fits with R-squared above 0.8 and mean absolute percentage error below 1. RNA half-lives were calculated as follows: $t_{1/2} = ln2/k_{decay}$. The final list of destabilized targets contains genes whose half-lives were calculated in all three KD conditions (luciferase, Nup98/96, and Nup107) and whose expression was decreased by at least 40% in the Nup98/96 KD compared to the luciferase KD, and also by at least 20% in the Nup98/96 KD compared to the Nup107 KD.

Total RNA-sequencing and miRNA enrichment analysis

Cells were seeded in 6 well plates and transfected with siRNA for 6 hours. RNA was isolated using Trizol (Ambion) and purified with the miRNeasy kit (Qiagen). Libraries were prepared using the TruSeq stranded total RNA kit (Illumina), and run on the Illumina NextSeq system (paired end 75).

After quality check and trimming, sequencing data was aligned to human reference sequence GRCh38 (hg38) and annotated with the corresponding gencode GTF file using the genome aligner STAR. To distinguish transcriptional and post-transcriptional targets, the number of exonic and intronic reads per gene was calculated using featureCounts (from Rsubread package). After filtering out low expression genes, differential expression was assessed using DESeq2. Transcriptional targets show a statistically significant (p-value <0.05) reduction in both intronic and exonic reads of at least 50%, while post-transcriptional targets show a statistically significant reduction (p-value < 0.05 and fold-change < 0.5) in only exonic reads.

The miRvestigator web application was used to analyze the 3' UTRs of the genes post-transcriptionally regulated at 6 hours post siRNA transfection. Overrepresented sequence motifs were detected using Weeder and these motifs were compared with the miRNA seed sequences available on miRBase to identify candidate miRNAs (Plaisier *et al.,* 2011).

miRNA mimics and inhibitors

Cells were co-transfected with the indicated siRNA and miRNA mimic for 24 hours and collected for qPCR as described in Chapter 2. Two different transfection protocols were used for the miRNA inhibitors. For the hsa-miR-218 inhibitor, cells were co-transfected with the indicated siRNA and miRNA inhibitor for 24 hours. For the hsa-miR-636 inhibitor, cells were

first transfected with the indicated siRNA for 24 hours, followed by a second transfection of the miRNA inhibitor for an additional 24 hours. Cells were collected and processed for qPCR as described in Chapter 2. The miRNA mimics and inhibitors used are listed in Table 3.4.

miRNA biotin immunoprecipitation

Cells were transfected with miRNA mimics (3' biotin tag) custom ordered from Dharmacon, and are listed in Table 3.4. miRNA mimics were based on the mature miRNA sequences for cel-miR-67 and hsa-miR-636. 48 hours after transfection, cells were resuspended in lysis buffer (20 mM Tris (pH 7.5), 100 mM KCl, 5 mM MgCl2, 0.3% NP-40, 50 U of RNase OUT (Invitrogen), complete mini-protease inhibitor cocktail (Roche Applied Sciences)) and incubated with Dynabeads MyOne Streptavidin C1 (Thermo Fisher Scientific) for 2 hours at 4° C with rotation. RNA was isolated using Trizol (Ambion) and purified with ethanol precipitation. cDNA synthesis and qPCR were performed as described in Chapter 2. Fold binding = X/Y, where X = miR IP/control IP, and Y = miR input/control input.

Ago2 immunoprecipitation and TaqMan miRNA qPCR

Cells were transfected with the indicated siRNA for 4 hours, and lysed in gentle hypotonic lysis buffer for 10 minutes on ice (10 mM Tris-HCl pH 7.5, 150 mM NaCl, 2 mM EDTA, 0.1% Triton-X100, 50 U of RNase OUT (Invitrogen), complete mini-protease inhibitor cocktail (Roche Applied Sciences)). The cell lysates were centrifuged at 14,000 RPM for 15 minutes at 4° C prior to incubation with Dynabeads M-280 sheep anti-rabbit IgG (Thermo Fisher Scientific: 11203D).

Dynabeads were prepared by blocking the beads with 0.5% BSA in PBS for 30 minutes, and conjugating the beads to 5 ug of Ago2 (Abcam, EPR10411) or rabbit IgG control (R&D Systems, AB-105-C) antibodies for 2 hours with rotation at 4° C. Dynabeads were washed twice with gentle hypotonic lysis buffer and incubated with the cell lysate for 2 hours with rotation at 4° C. After incubation with the cell lysate, Dynabeads were washed 5 times with NET-2 buffer (50 mM Tris-HCl pH 7.5, 150 mM NaCl, 0.05% Triton-X100). 10% of the beads were prepared for western blot analysis by boiling the beads in 1x sample buffer for 5 minutes. 90% of the beads were prepared for RNA isolation using Trizol (Ambion).

miRNA expression was quantified using the TaqMan miRNA assay (Thermo Fisher Scientific, 4427975), prepared according to the manufacture's instructions. Reverse transcription and TaqMan small RNA mixes used were specific for hsa-RNU66 (Assay ID: 001002), hsa-miR-17 (Assay ID: 002308), and hsa-miR-636 (Assay ID: 002088). 5 ng of total RNA was used for hsa-miR-17 reverse transcription, and 10 ng of total RNA was used for hsa-RNU66 and hsa-miR-636 reverse transcription. Fold enrichment = $2^{-(\text{Ct Ago2 IP - Ct IgG IP})}$.

a.

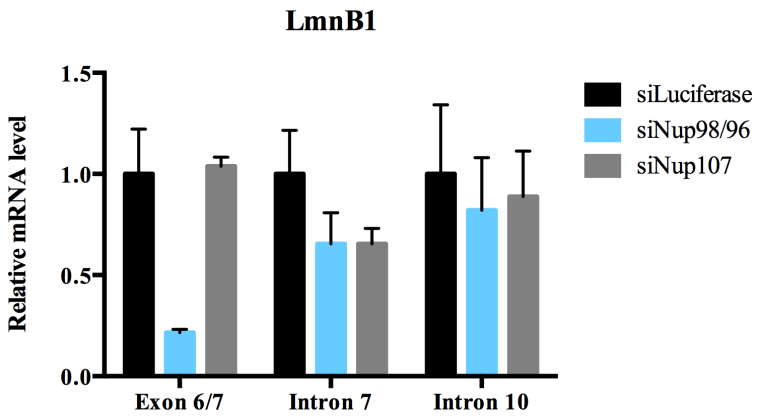

b.

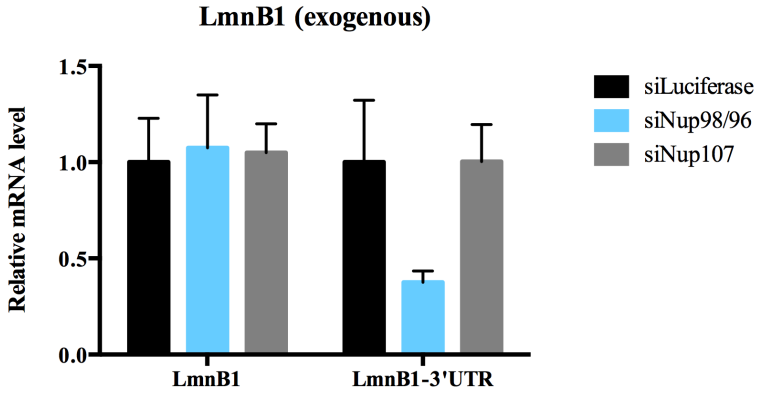

Figure 3.1. LmnB1 mRNA is post-transcriptionally regulated through its 3' UTR upon Nup98/96 knockdown

a. U2OS cells were treated with the indicated siRNA for 48 hours and expression of Lamin B1 pre-mRNA (intron 7 and intron 10) and Lamin B1 mature mRNA (exon 6/7) were quantified using qPCR. Intron 7 and intron 10 primers span an intron and the following exon. Exon 6/7 primers, recognizing the spliced transcript, span an exon-exon junction. Relative mRNA levels normalized to RPL4 are plotted. Error bars were computed as standard deviation over three biological replicates. b. RPE1 cells expressing exogenous LmnB1 or LmnB1 with its 3' UTR were treated with the indicated siRNA for 48 hours. Expression of the exogenous construct was quantified by qPCR, and relative mRNA levels normalized to RPL4 are plotted. Error bars were computed as standard deviation over three biological replicates.

a.

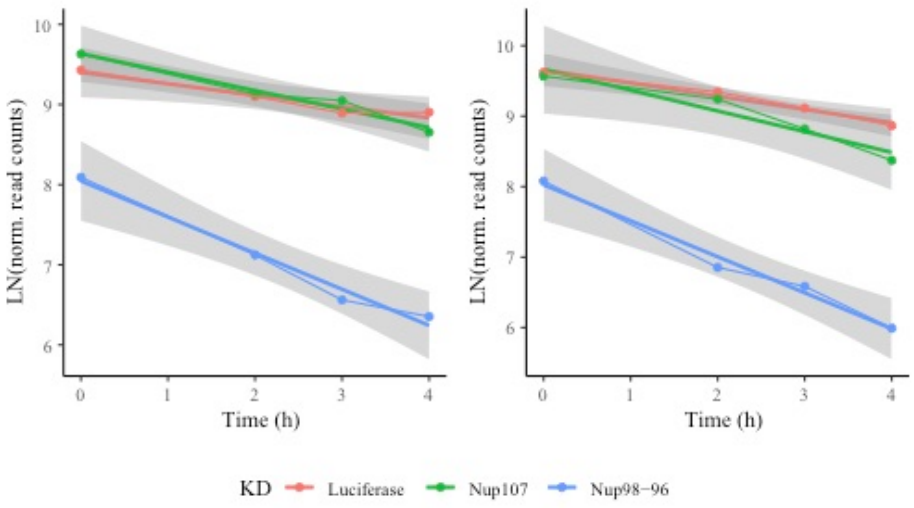

b.

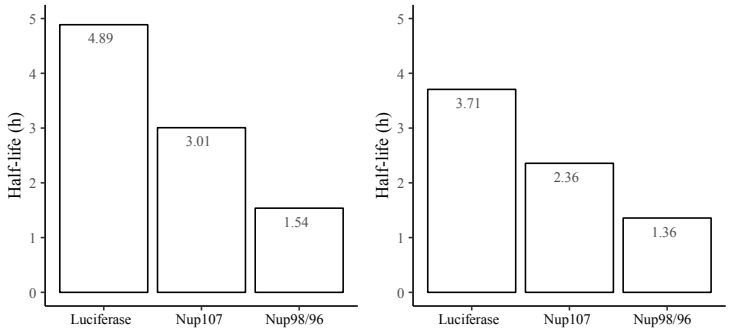

Figure 3.2. LmnB1 mRNA is destabilized upon Nup98/96 knockdown
U2OS cells were transfected with the indicated siRNA for 48 hours and treated with Actinomycin D (5 ug/mL). Cells were collected at 0, 2, 3, and 4 hours after Actinomycin D treatment, and libraries were prepared for RNA-sequencing. LmnB1 read counts normalized to a yeast spike-in control are plotted over the time course (a), and the estimated mRNA half life calculations for LmnB1 are shown (b).

a.

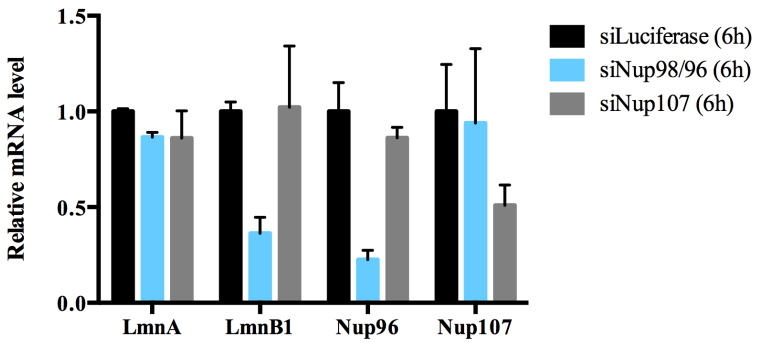

b.

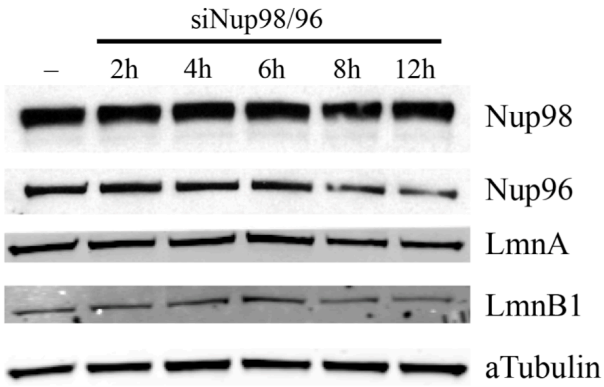

Figure 3.3. LmnB1 mRNA expression correlates with Nup98/96 mRNA expression, not protein expression

a. U2OS cells treated with the indicated siRNA for 6 hours were processed for qPCR analysis of LmnA, LmnB1, Nup96 and Nup107 mRNA expression. Relative mRNA levels normalized to RPL4 are plotted. Error bars were computed as standard deviation over three biological replicates. b. U2OS cells treated with Nup98/96 siRNA for 0, 2, 4, 6, 8, or 12 hours were processed to analyze Nup98, Nup96, LmnA, and LmnB1 protein expression by western blot.

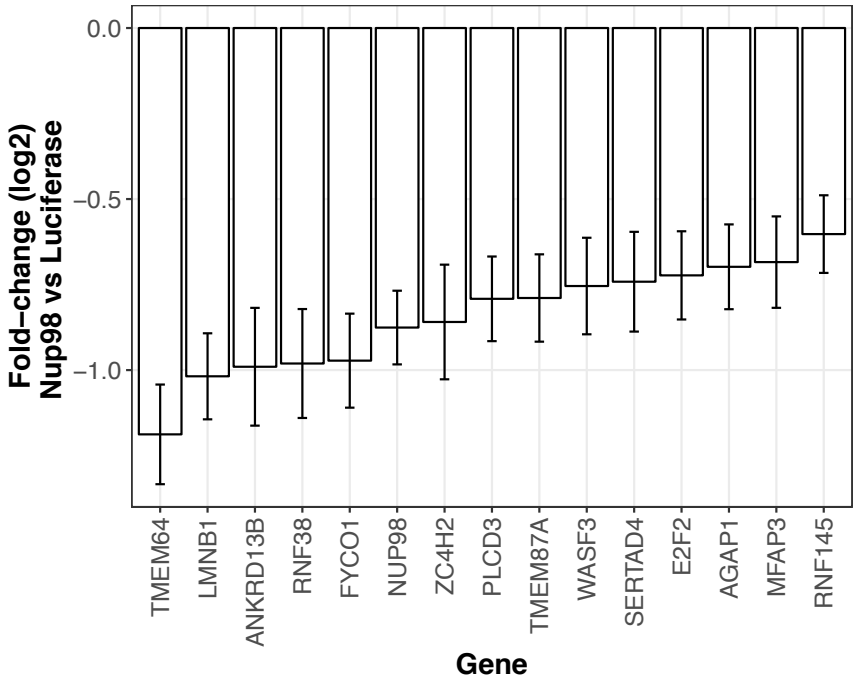

Figure 3.4. Top 15 genes post-transcriptionally regulated at 6 hours post Nup98/96 siRNA transfection

U2OS cells were treated with luciferase, Nup98/96, or Nup107 siRNA oligonucleotides for 6 hours and prepared for total RNA-sequencing. The number of exonic and intronic reads per gene was calculated, and post-transcriptional targets show a statistically significant reduction (p-value < 0.05 and fold-change < 0.5) in only exonic reads. The top 15 post-transcriptional target genes specific to the Nup98/96 KD condition are shown.

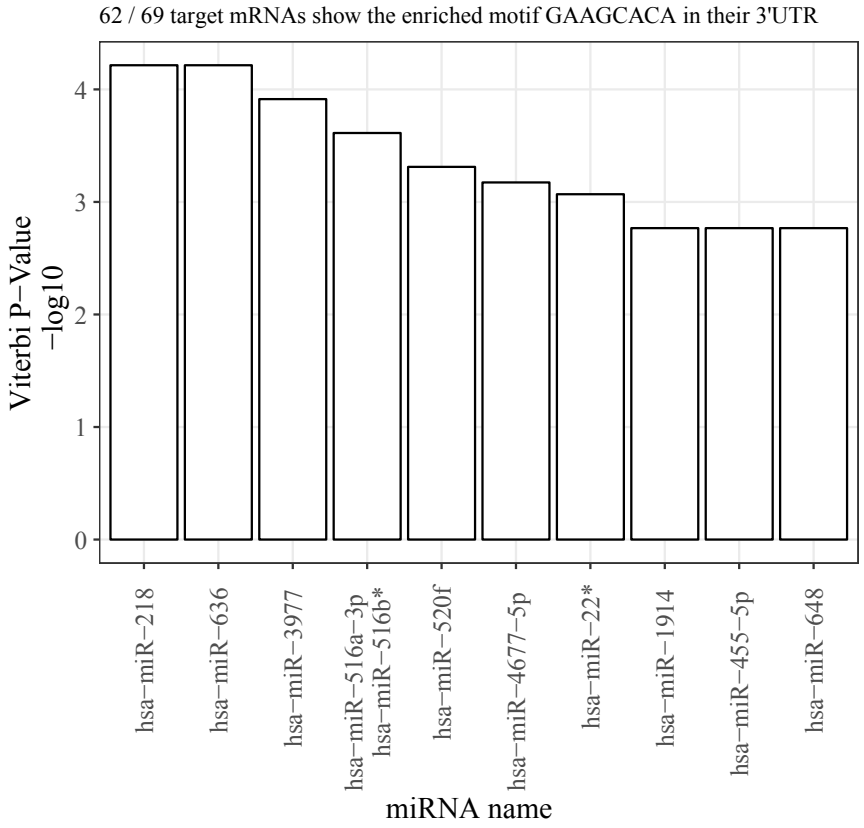

Figure 3.5. Top 10 miRNAs predicted to target the enriched GAAGCACA motif in the 3' UTR of genes post-transcriptionally regulated at 6 hours post Nup98/96 siRNA transfection
The 69 genes post-transcriptionally regulated at 6 hours post Nup98/96 siRNA transfection were analyzed for overrepresented sequence motifs in their 3' UTRs using the miRvestigator web application. The identified motif was compared with miRNA seed sequences available on miRBase, and candidate miRNAs are listed.

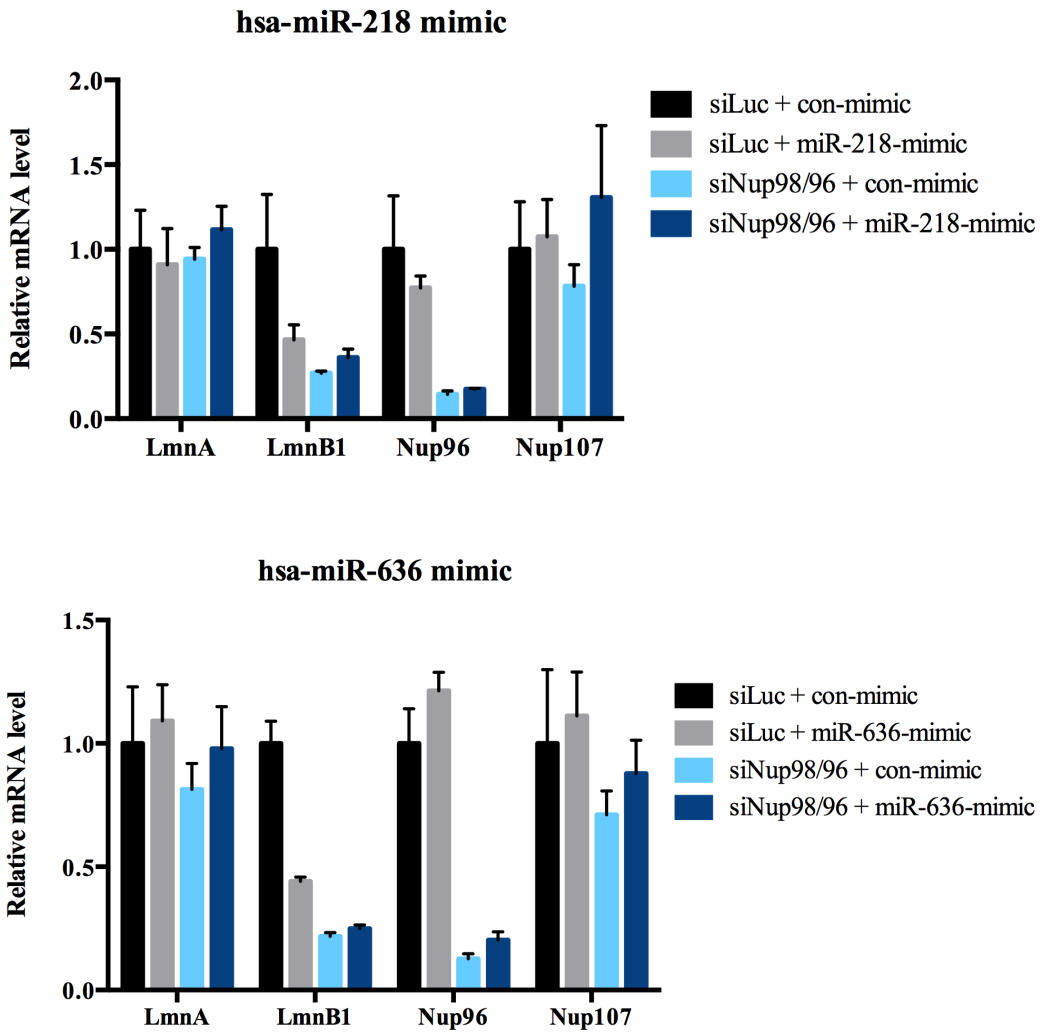

Figure 3.6. hsa-miR-218 and hsa-miR-636 regulate LmnB1 mRNA expression
U2OS cells were co-transfected with the indicated siRNA and miRNA mimic for 24 hours and mRNA expression of LmnA, LmnB1, Nup96, and Nup107 were analyzed by qPCR. Relative mRNA levels normalized to RPL4 are plotted. Error bars were computed as standard deviation over three biological replicates.

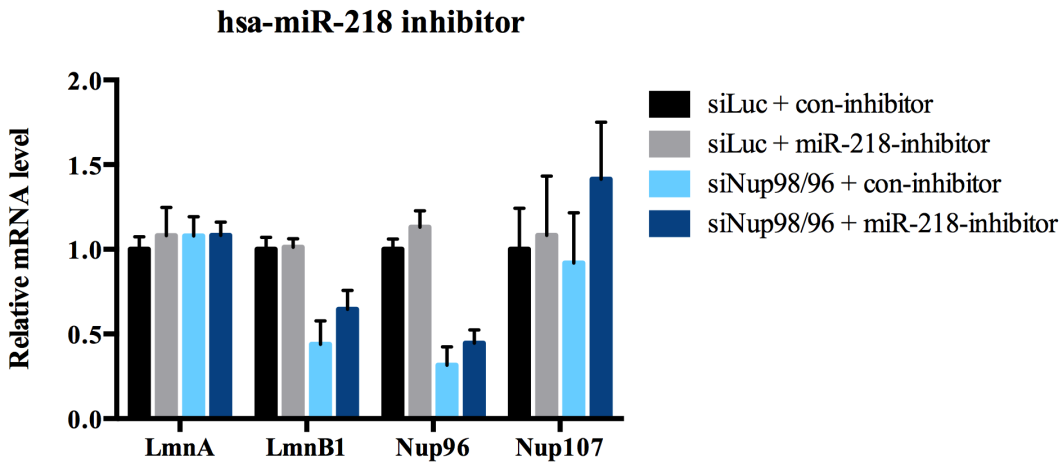

Figure 3.7. hsa-miR-218 inhibitors do not protect LmnB1 mRNA from degradation upon Nup98/96 siRNA transfection

U2OS cells were co-transfected with the indicated siRNA and miRNA inhibitor for 24 hours and mRNA expression of LmnA, LmnB1, Nup96, and Nup107 were analyzed by qPCR. Relative mRNA levels normalized to RPL4 are plotted. Error bars were computed as standard deviation over three biological replicates.

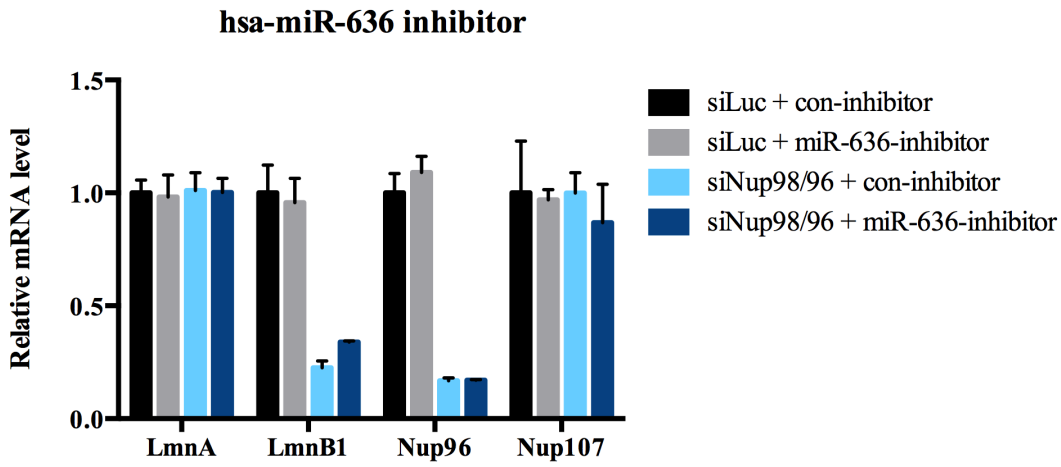

Figure 3.8. hsa-miR-636 inhibitors partially protect LmnB1 mRNA from degradation upon Nup98/96 siRNA transfection

U2OS cells were transfected with the indicated siRNA for 24 hours, followed by a second transfection of the miRNA inhibitor for an additional 24 hours. mRNA expression of LmnA, LmnB1, Nup96, and Nup107 were analyzed by qPCR. Relative mRNA levels normalized to RPL4 are plotted. Error bars were computed as standard deviation over three biological replicates.

a.

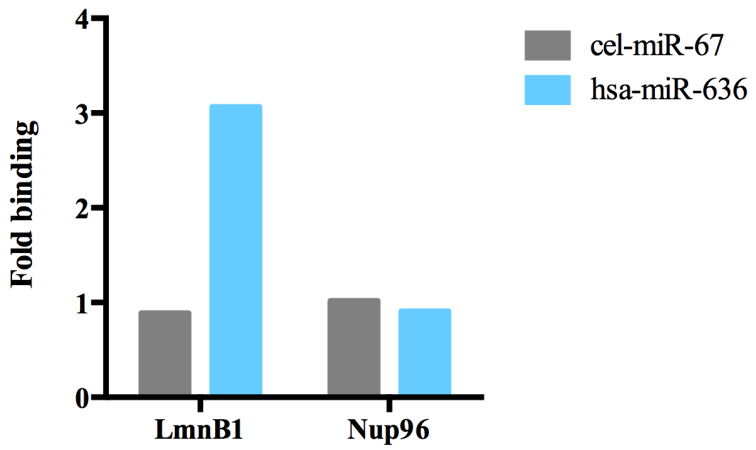

b.

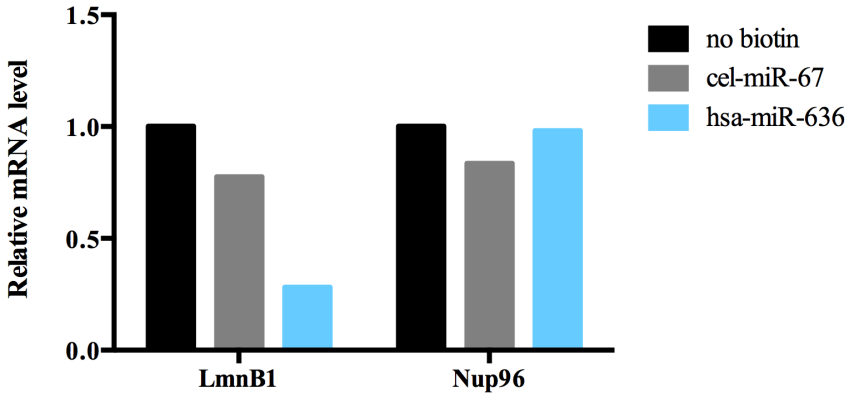

Figure 3.9. hsa-miR-636 binds LmnB1 mRNA, but not Nup98/96 mRNA
U2OS cells were transfected with the indicated 3' biotin tagged miRNA mimic for 48 hours. miRNA mimics were isolated from 90% of the cell lysate, and qPCR was used to assess enrichment for LmnB1 and Nup98/96 mRNA (a). Fold binding = X/Y, where X = miR IP/control IP, and Y = miR input/control input. The remaining 10% of the cell lysate was used to quantify the expression of LmnB1 and Nup98/96 in each condition (b). Relative mRNA levels normalized to RPL4 are plotted.

a.

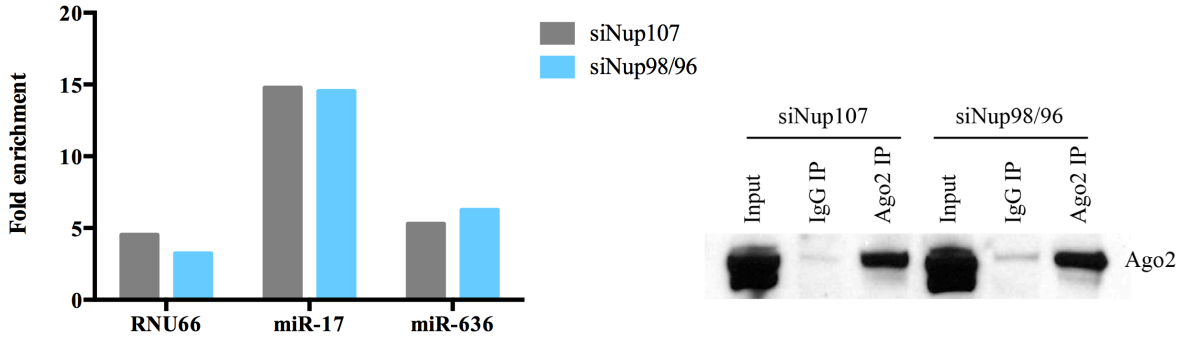

b.

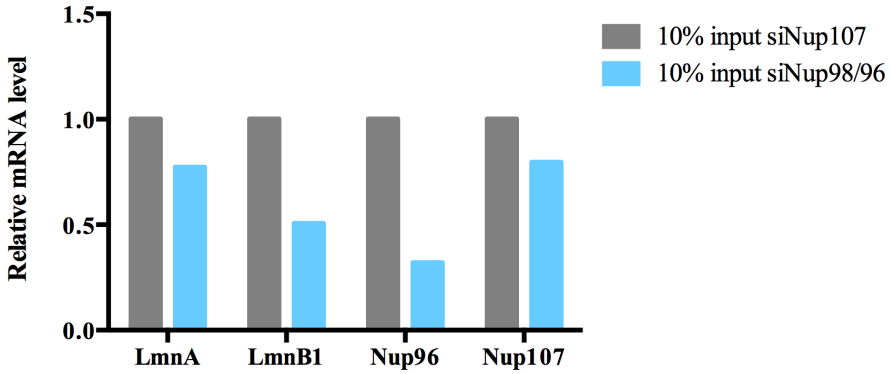

Figure 3.10. hsa-miR-636 is not preferentially loaded into the RISC upon Nup98/96 siRNA transfection

a. U2OS cells were transfected with the indicated siRNA for 4 hours, followed by Ago2 immunoprecipitation. miRNA expression in the Ago2 pulldown fraction was quantified using the TaqMan miRNA assay. Fold enrichment = $2^{-(Ct\ Ago2\ IP\ -\ Ct\ IgG\ IP)}$. Confirmation of Ago2 immunoprecipitation by western blot is shown. b. 10% of the total cell lysate was used to confirm Nup98/96 KD by qPCR, and relative mRNA levels normalized to RPL4 are plotted.

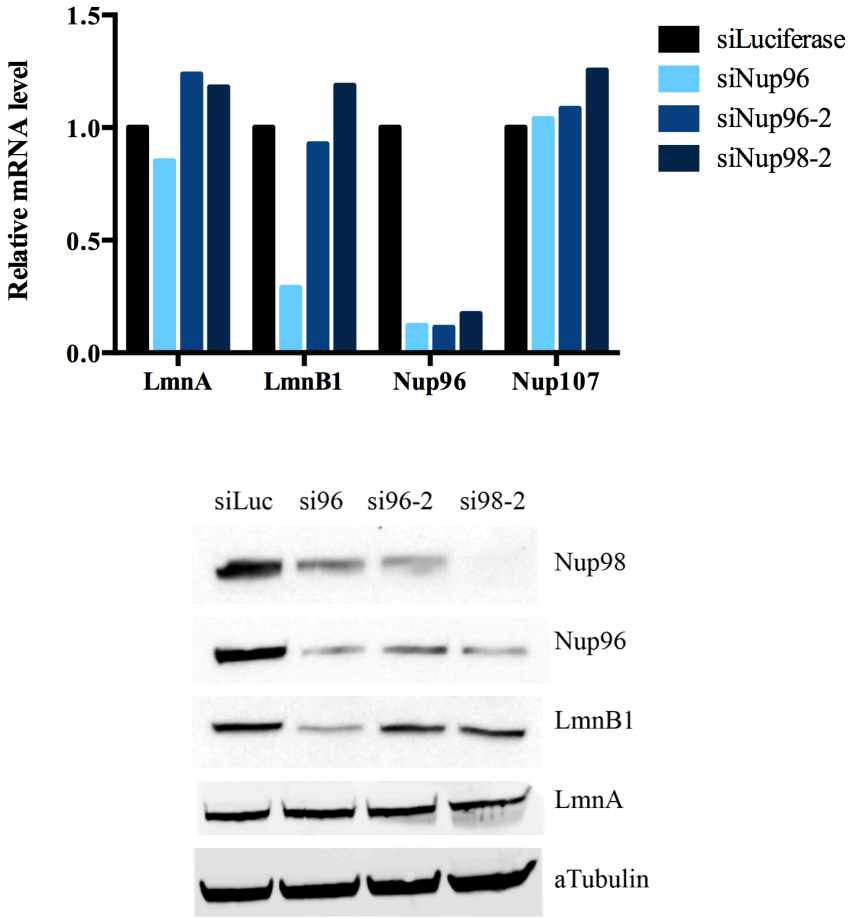

Figure 3.11. Newly designed Nup98/96 siRNA oligonucleotides do not regulate LmnB1 mRNA or protein expression
U2OS cells were transfected with the indicated siRNA for 48 hours and mRNA (top) or protein (bottom) expression were analyzed by qPCR and western blot, respectively. Relative mRNA levels normalized to RPL4 are plotted.

Table 3.1. Estimated half lives for destabilized genes at 48 hours post Nup98/96 siRNA transfection

U2OS cells were transfected with the indicated siRNA for 48 hours and treated with Actinomycin D (5 ug/mL) to monitor mRNA decay. The genes destabilized specifically in the Nup98/96 KD condition are listed based on their change in stability, with the most destabilized target genes at the top.

Gene	Half-life (hours)					
	siLuc Rep1	siLuc Rep2	si107 Rep1	si107 Rep2	si96 Rep1	si96 Rep2
LMNB1	4.89	3.71	3.01	2.36	1.54	1.36
JPT1	4.01	3.08	3.49	2.51	1.29	1.23
APOPT1	6.36	3.85	3.84	2.32	2.10	1.63
RNF145	5.48	3.07	2.40	2.24	1.72	1.46
MRPS27	4.52	2.95	2.70	2.03	1.85	1.57
CDH2	7.12	5.86	4.25	3.42	3.39	2.75
CZ4H2	5.51	4.88	4.10	3.13	3.12	1.88
ARL13B	3.89	2.55	2.44	2.08	1.82	1.38
RASGEF1A	3.41	3.62	2.56	2.11	1.99	1.67
CENPB	2.65	2.47	2.03	1.68	1.47	1.25

Table 3.2. List of genes post-transcriptionally regulated at 6 hours post Nup98/96 siRNA transfection

U2OS cells were treated with luciferase, Nup98/96, or Nup107 siRNA oligonucleotides for 6 hours and prepared for total RNA-sequencing. The number of exonic and intronic reads per gene was calculated, and post-transcriptional targets show a statistically significant reduction (p-value < 0.05 and fold-change < 0.5) in only exonic reads. Genes post-transcriptionally regulated specifically upon Nup98/96 KD are listed.

Gene	si98 vs siLuc			si98 vs si107		
	log2FoldChange	lfcSE	padj.	log2FoldChange	lfcSE	padj.
TMEM64	-1.187958268	0.145671223	4.56E-14	-1.219074821	0.153595309	7.14E-13
LMNB1	-1.018211346	0.125775964	3.54E-13	-1.144825782	0.130600326	5.47E-14
ANKRD13B	-0.990298525	0.172170051	1.10E-06	-0.448226305	0.419289013	0.003042995
RNF38	-0.980783907	0.159248356	5.08E-08	-0.256808115	0.348068375	0.001355732
FYCO1	-0.972451207	0.137441119	1.47E-10	-0.576545597	0.272052648	1.31E-04
ELOVL7	-0.88338812	0.218011591	5.99E-04	-0.360207413	0.467692914	0.008303212
NUP98	-0.875699223	0.107700788	2.32E-13	-0.873830693	0.11091639	2.03E-12
ZC4H2	-0.859398233	0.167589775	2.69E-05	-1.060206673	0.179603458	1.41E-06
PLCD3	-0.791696358	0.123704323	3.05E-08	-0.741707015	0.133160514	7.14E-07
TMEM87A	-0.789281628	0.127674131	1.75E-07	-0.943710618	0.132873461	3.80E-10
MOSPD1	-0.756599596	0.162855303	2.19E-04	-0.965084552	0.171684697	5.18E-06
WASF3	-0.754292034	0.141112106	2.00E-05	-0.345192027	0.331019912	0.004139096
SERTAD4	-0.741653192	0.145801357	2.99E-05	-0.712720373	0.223388916	4.70E-05
E2F2	-0.723108606	0.128923984	4.16E-06	-0.66934028	0.170208398	2.21E-05
AGAP1	-0.698108083	0.123952383	3.10E-06	-0.629427585	0.170508198	2.53E-05
AL159978.1	-0.685078636	0.187255155	0.001777806	-0.109939414	0.25069909	0.018921452
MFAP3	-0.684372529	0.13364889	3.07E-05	-0.689533174	0.176686332	1.89E-05
SNX4	-0.676258533	0.137047663	7.05E-05	-0.766163917	0.153339859	4.03E-06
ARL13B	-0.659296495	0.132166612	5.14E-05	-0.818864263	0.138527236	2.68E-07
EPS8	-0.654499477	0.168386233	0.001067213	-1.000298032	0.159211338	2.76E-07
ZNF367	-0.652520686	0.132736208	6.25E-05	-0.903419551	0.136927178	9.46E-09
MOCS2	-0.646571752	0.137994849	1.25E-04	-0.578402316	0.254928548	1.29E-04
NUDT10	-0.641854598	0.138849349	1.54E-04	-0.627948803	0.226892004	8.20E-05
HMOX1	-0.636470058	0.127114174	5.14E-05	-0.017189765	0.074444393	0.02549842
MKRN1	-0.624089931	0.121800949	3.41E-05	-0.777950078	0.127387223	9.88E-08
RNF220	-0.618270802	0.123940302	5.49E-05	-0.764344199	0.129968853	2.76E-07
LRIG1	-0.614053351	0.141405102	0.00059337	-0.316777433	0.310641049	0.00354042
STX2	-0.610417148	0.126855781	1.23E-04	-0.808930823	0.130773471	5.96E-08
RNF145	-0.602456563	0.113443736	2.00E-05	-0.674688603	0.121848278	8.41E-07
LIN28B	-0.584733589	0.17392438	0.001598777	-0.887892754	0.151472706	3.18E-07
BEND3P1	-0.582707432	0.167926602	0.002101411	-0.668381092	0.228057168	4.19E-04
SFMBT1	-0.581972344	0.116619416	7.07E-05	-0.61056324	0.14294406	1.37E-05
ATG16L1	-0.55984061	0.110072837	4.62E-05	-0.667547439	0.116668098	3.73E-07
UBE2Q2	-0.55574581	0.178243067	0.002101411	-0.359751215	0.327074372	5.64E-04
KLHL11	-0.553213995	0.134383801	5.69E-04	-0.68299293	0.142438086	5.25E-06
ARAF	-0.544430406	0.12438867	3.49E-04	-0.499266201	0.218912277	1.22E-04
ARHGEF12	-0.515719263	0.118110924	4.76E-04	-0.24079756	0.248094222	8.36E-04
ICK	-0.506683518	0.213415457	0.00769645	-0.115249294	0.234498039	0.016380581
AP1M1	-0.503828884	0.128913419	8.09E-04	-0.077519659	0.167293166	0.004138579
DLD	-0.492836601	0.18361342	0.003616736	-0.28208788	0.298537997	6.94E-04
APPL2	-0.489783324	0.214073225	0.008446674	-0.363448545	0.32978843	0.003042995
AFMID	-0.484596853	0.178292245	0.003616736	-0.44234341	0.282900366	6.94E-04

Table 3.2. List of genes post-transcriptionally regulated at 6 hours post Nup98/96 siRNA transfection, continued

Gene	si98 vs siLuc			si98 vs si107		
	log2FoldChange	lfcSE	padj.	log2FoldChange	lfcSE	padj.
JPT1	-0.481643029	0.138676031	0.002361097	-0.622371559	0.135998629	2.16E-04
SLC45A3	-0.481532392	0.224276915	0.011688149	-0.074475903	0.190006731	0.02549842
VAMP3	-0.474695017	0.13152974	0.001161702	-0.261696024	0.250901963	6.80E-04
KLHL12	-0.466870681	0.158806721	0.003632636	-0.446650902	0.247813091	2.01E-04
TUB	-0.457514794	0.160559158	0.003119904	-0.470787444	0.233839515	1.52E-04
DESI2	-0.444246199	0.257641612	0.01632361	-0.159098039	0.278844	0.002391399
CPOX	-0.444091546	0.168496673	0.004003249	-0.614025341	0.152477424	1.55E-05
TRIM23	-0.436927056	0.247027712	0.010575763	-0.295398508	0.331389437	8.36E-04
SYPL1	-0.412486522	0.299718749	0.021451409	-0.023862128	0.111725651	0.020313814
USP32	-0.409820714	0.161384661	0.004463232	-0.023921499	0.0841447	0.017162327
MRPS27	-0.404900568	0.138895326	0.003119904	-0.541619004	0.12474832	1.24E-05
BAHD1	-0.402441271	0.205074265	0.008446674	-0.010978159	0.053048138	0.049322075
KIF2A	-0.394334966	0.222614203	0.014509792	-0.01841936	0.079647279	0.024396284
AC006441.3	-0.379999876	0.198001129	0.008323947	-0.033903652	0.109366304	0.012165015
C5orf15	-0.377475123	0.198529693	0.011811422	-0.387594394	0.262333912	3.81E-04
NT5C3A	-0.368134199	0.285423062	0.019718211	-0.151380255	0.281224324	0.002578191
TMEM9B	-0.351734207	0.216944473	0.012915094	-0.132887383	0.22321896	0.001912454
LASP1	-0.336849364	0.171742757	0.011688149	-0.013079148	0.051698362	0.03933485
MFN2	-0.329243297	0.174877273	0.013632452	-0.333722257	0.222932746	3.66E-04
CENPB	-0.298657598	0.230966227	0.021451409	-0.078795389	0.178339645	0.004139096
HSPA14	-0.243196135	0.197656554	0.030342226	-0.445912624	0.189011566	1.24E-04
SLC39A11	-0.233167906	0.228991468	0.042953553	-0.29914874	0.284874108	6.94E-04
SLC37A3	-0.214764271	0.237700898	0.041686182	-0.025846983	0.10050795	0.01672399
FAM104A	-0.212168711	0.195449083	0.036556272	-0.012885662	0.051641363	0.039967173
TAF11	-0.209303611	0.216619805	0.047054078	-0.426865812	0.251294315	2.51E-04
TNFRSF10B	-0.204485363	0.199619641	0.048915427	-0.148086553	0.21019965	0.001912454
CERK	-0.180456668	0.209510049	0.04485339	-0.527486872	0.202072049	1.01E-04

Table 3.3. Sequence comparisons between Nup98/96 siRNA oligonucleotides and miRNAs hsa-miR-218 and hsa-miR-636

Oligonucleotide sequences for each siRNA and miRNA are listed, and seed sequence similarities are underlined.

Antisense siRNA or mature miRNA name	**Sequence (5'-3')**
siNup96	AGUGCUUCACAAUUUGUGC
siNup96-2	UAUUCUGAAAUGCUUCUUC
siNup98	UUGCUUAGGAAACUAAAUCUCUCUC
siNup98-2	AUUCCCACUGGUAUUUGUG
hsa-miR-218	UUGUGCUUGAUCUAACCAUGU
hsa-miR-636	UGUGCUUGCUCGUCCCGCCCGCA

Table 3.4. List of miRNA mimics and inhibitors – Chapter 3

miRNA mimic or inhibitor name	Dharmacon product number	Final concentration
miRNA mimic negative control	CN-001000-01	100 nM
miRNA inhibitor negative control	IN-001005-01	100 nM
hsa-miR-218 mimic	C-300574-03	100 nM
hsa-miR-218 inhibitor	IH-300574-05	100 nM
hsa-miR-636 mimic	C-300963-03	100 nM
hsa-miR-636 inhibitor	IH-300963-04	100 nM
cel-miR-67 mimic (3' biotin tag)	Custom order	200 nM
hsa-miR-636 mimic (3' biotin tag)	Custom order	200 nM
hsa-miR-636:LmnB1 target site protector	Custom order	50 nM

Acknowledgements

We thank Juliana S. Capitanio for help with the mRNA half-life analysis, intron-exon analysis for post-transcriptionally deregulated targets, and miRNA binding site analysis; and the Salk Next Generation Sequencing core for sequencing our cDNA libraries, and preparing libraries for total RNA-sequencing.

Chapter 3 is unpublished material coauthored with Capitanio, Juliana S. The dissertation author, under guidance of Martin W. Hetzer, was the primary researcher and author of this material.

References

Filipowicz, W., Bhattacharyya, S. N., & Sonenberg, N. Mechanisms of post-transcriptional regulation by microRNAs: are the answers in sight?. *Nat. Rev. Genetics.* **9**, 102–114 (2008).

Hausser, J., Syed, A. P., Bilen, B., & Zavolan, M. Analysis of CDS-located miRNA target sites suggests that they can effectively inhibit translation. *Genome Res.* **23**, 604–615 (2013).

Jackson, A. L., Burchard, J., Schelter, J., Chau, B. N., Cleary, M., Lim, L., & Linsley, P. S. Widespread siRNA "off-target" transcript silencing mediated by seed region sequence complementarity. *RNA*. **12**, 1179–1187 (2006).

Li, S. P., Xu, H. X., Yu, Y., He, J. D., Wang, Z., Xu, Y. J., Wang, C. Y., Zhang, H. M., Zhang, R. X., Zhang, J. J., Yao, Z., & Shen, Z. Y. LncRNA HULC enhances epithelial-mesenchymal transition to promote tumorigenesis and metastasis of hepatocellular carcinoma via the miR-200a-3p/ZEB1 signaling pathway. *Oncotarget.* **7**, 42431–42446 (2016).

Lin, S. T., & Fu, Y. H. miR-23 regulation of lamin B1 is crucial for oligodendrocyte development and myelination. *Dis. Model Mech.* **2**, 178–188 (2009).

Lin, X., Ruan, X., Anderson, M. G., McDowell, J. A., Kroeger, P. E., Fesik, S. W., & Shen, Y. siRNA-mediated off-target gene silencing triggered by a 7 nt complementation. *Nucleic Acids Res*. **33**, 4527–4535 (2005).

Lytle, J. R., Yario, T. A., & Steitz, J. A. Target mRNAs are repressed as efficiently by microRNA-binding sites in the 5' UTR as in the 3' UTR. *Proc. Nati. Acad. Sci. USA*. **104**, 9667–9672 (2007).

Plaisier, C. L., Bare, J. C., & Baliga, N. S. miRvestigator: web application to identify miRNAs responsible for co-regulated gene expression patterns discovered through transcriptome profiling. *Nucleic Acids Res*. **39**, W125–W131 (2011).

Poliseno, L., Salmena, L., Zhang, J., Carver, B., Haveman, W. J., & Pandolfi, P. P. A coding-independent function of gene and pseudogene mRNAs regulates tumour biology. *Nature*. **465**, 1033–1038 (2010).

Salmena, L., Poliseno, L., Tay, Y., Kats, L., & Pandolfi, P. P. A ceRNA hypothesis: the Rosetta Stone of a hidden RNA language?. *Cell.* **146**, 353–358 (2011).

Seitz H. Redefining microRNA targets. *Curr. Biol.* **19**, 870–873 (2009).

Setijono, S. R., Park, M., Kim, G., Kim, Y., Cho, K. W., & Song, S. J. miR-218 and miR-129 regulate breast cancer progression by targeting Lamins. *Biochem. Biophys. Res. Commun.* **496**, 826–833 (2018).

Tay, Y., Kats, L., Salmena, L., Weiss, D., Tan, S. M., Ala, U., Karreth, F., Poliseno, L., Provero, P., Di Cunto, F., Lieberman, J., Rigoutsos, I., & Pandolfi, P. P. Coding-independent regulation of the tumor suppressor PTEN by competing endogenous mRNAs. *Cell*. **147**, 344–357 (2011).

Chapter 4: Lamin B1 overexpression alters chromatin organization and gene expression

Introduction

Proper gene expression is critical for cells to maintain their identity and function, and the organization of chromatin within the nucleus is one of the main factors influencing gene expression. The conventional pattern of chromatin organization places highly transcribed euchromatic regions of the genome within the nucleoplasm, and gene poor, transcriptionally repressed heterochromatic regions at the nuclear periphery (Buchwalter *et al.,* 2018). However, in rare cases an inverted pattern is observed, with euchromatin localized at the nuclear periphery and heterochromatin within the nucleoplasm. This occurs specifically in the rod photoreceptor cells of nocturnal animals, and was proposed to be an adaptation for night vision (Solovei *et al.,* 2009).

Altered chromatin organization is also observed during normal and pathological aging. Heterochromatin is lost from the nuclear periphery, and in some cases, form heterochromatic foci within the nucleoplasm, called senescence associated heterochromatin foci (SAHF) (Goldman *et al.,* 2004; McCord *et al.,* 2013; Narita *et al.,* 2003). SAHF are suggested to sequester and inhibit the transcription of specific genes, such as E2F targets required for cell proliferation, to promote and maintain the senescent state (Narita *et al.,* 2003).

All of these reported changes in chromatin organization are associated with aberrant expression of a single or combination of nuclear envelope (NE) proteins, including lamin B receptor (LBR), LmnA, and LmnB1 (Solovei *et al.,* 2013; Goldman *et al.,* 2004; McCord *et al.,* 2013). Downregulation of both LBR and LmnA mediates the inverted chromatin organization observed in mouse rod photoreceptor cells, and downregulation of LmnB1 is associated with SAHF formation in aging and senescence induction (Solovei *et al.,* 2013; Shimi *et al.,* 2011; Sadaie *et al.,* 2013; Shah *et al.,* 2013; Chandra *et al.,* 2015). However, expression of mutant

LmnA in Hutchinson-Gilford progeria syndrome, a premature aging disorder, increases the thickness of the lamina and reduces heterochromatin at the nuclear periphery (Goldman *et al.,* 2004; McCord *et al.,* 2013). This demonstrates that modulating NE protein levels can have profound effects on 3D chromatin organization.

In line with this, we and a few others observed that LmnB1 overexpression (OE) alters chromatin organization, resembling SAHF, in epithelial and fibroblast cells (Lin and Fu, 2009; Barascu *et al*., 2012). This would suggest that LmnB1 OE induces senescence, and some studies have shown senescence induction upon LmnB1 OE (Barascu *et al.,* 2012; Dreesen *et al.,* 2013). However, this contradicts numerous studies showing that various inducers of senescence downregulate LmnB1, and LmnB1 KD induces senescence (Freund *et al.,* 2012; Shimi *et al.,* 2011; Shah *et al.,* 2013). Further, SAHF-like structures have also been observed in proliferating cells expressing oncogenic H-RasV12 and deficient in the DNA damage response, and also human tumor samples. This heterochromatin formation did not prevent the transcription of E2F target genes, but rather appeared to function in impairing DNA damage response signaling and apoptosis (Di Micco *et al.,* 2011).

It is not clear how or why LmnB1 OE alters chromatin organization, or whether LmnB1 OE induces senescence-like phenotypes. This will be the focus of the following chapter, and may have interesting applications in the context of diseases that exhibit high expression of LmnB1, including a variety of neurological diseases and cancer (Alcalá-Vida *et al.,* 2021; Barascu *et al.,* 2012; Padiath *et al.,* 2006; Sun *et al.,* 2010; Yi *et al.,* 2020).

Results

LmnB1 overexpression alters chromatin organization and gene expression

To study the changes associated with LmnB1 overexpression (OE), we established stable cell lines in epithelial cells (RPE1) and fibroblasts (IMR90s) that express mCherry-LmnB1 in the presence of doxycycline. In RPE1 cells, we isolated two clonal lines for each OE construct for downstream analyses. Using these cell lines, immunofluorescence imaging revealed that ~2 fold OE of LmnB1 in RPE1 and IMR90 cells alters chromatin organization, such that punctate DNA foci form within the nucleus (Figure 4.1). This was evident in >80% of cells overexpressing LmnB1, and was not observed upon OE of mutant LmnB1 (LmnB1-ΔCaaX), which is a 4 amino acid deletion that prevents the post-translational processing and insertion of LmnB1 into the nuclear envelope, or upon OE of inner nuclear membrane (INM) protein Lap2β. Further, LmnB1 OE induced changes in chromatin organization are reversible, as doxycycline removal leads to loss of these DNA foci within 48 hours (data not shown). This demonstrates the specificity of this phenotype for LmnB1, and its specific OE at the nuclear envelope.

These results were corroborated by electron microscopy imaging, which showed a stark reduction of heterochromatin associating with the nuclear envelope upon OE of LmnB1 (Figure 4.2). This led us to hypothesize that the DNA foci clustering within the nucleus may be heterochromatic in nature. Using immunofluorescence imaging for specific heterochromatin markers, we observed that these DNA foci colocalize with H3K9me3 and HP1, but not H3K27me3 (Figure 4.3). Further, we did not observe any global changes in the expression of these proteins by western blot (Figure 4.4).

Given the LmnB1 OE induced alterations in chromatin organization, we assessed whether these correlated with changes in gene expression. mRNA sequencing performed at 24 hours post

doxycycline induction identified hundreds of differentially expressed genes specific to LmnB1 OE, but these genes did not show any enrichment for biological pathways or transcription factor binding sites (Figure 4.5, data not shown). Taken together, our results suggest that modulating the levels of LmnB1 greatly impacts chromatin organization, and the differences in gene expression observed may be a consequence of changes in chromatin interactions, or alterations in the deposition of histone modification across the genome, such as H3K9me3.

LmnB1 overexpression affects the tethering of heterochromatin at the nuclear periphery

Our next goal was to determine the mechanism through which LmnB1 OE induces changes in chromatin organization. We hypothesized that LmnB1 OE may be affecting the targeting or tethering of heterochromatin at the NE. To test this, we assessed whether these heterochromatic DNA foci can form without NE reassembly following mitosis. We arrested cells in G1/S phase with aphidicolin for 24 hours, followed by doxycycline induction of LmnB1 and culturing with the thymidine analogue EdU for 24 hours. EdU was used to confirm that cells are not undergoing DNA synthesis while LmnB1 is being overexpressed. Using immunofluorescence imaging, we observed the formation of DNA foci colocalizing with H3K9me3 in more than 50% of arrested cells overexpressing LmnB1 (Figure 4.6). This demonstrated the independence of this phenotype from mitosis, and further suggests that the tethering of chromatin at the nuclear periphery is being compromised by LmnB1 OE.

We then checked the localization and expression of other lamin isoforms and INM proteins to determine whether these are altered and potentially affecting the proper localization of heterochromatin at the nuclear periphery. However, we observed no changes in these proteins, further supporting the specificity of the phenotype to LmnB1 OE, and suggesting that LmnB1

might be forming a physical barrier that prevents the binding of heterochromatin at the nuclear periphery (Figure 4.7).

LmnB1 overexpression slows cell proliferation but does not induce senescence

Finally, we wanted to determine whether LmnB1 OE induces senescence, given that the induced DNA foci have several characteristics in common with SAHF, and these cells show a decrease in cell proliferation (Figure 4.8). Using the CellEvent Senescence Green Detection Kit (Thermo Fisher Scientific), we did not observe any signs of senescence after 9 days of LmnB1 OE (Figure 4.9). RPE1 cells treated with doxorubicin showed clear induction of senescence at 9 days, demonstrating that these cells can become senescent despite hTERT expression. We also pulsed these cells in a separate experiment with EdU, and did not observe any halt in DNA replication (data not shown). Together, this clearly demonstrates that LmnB1 OE does not induce senescence, despite similarities in chromatin organization.

Discussion

Here we show that LmnB1 OE induces significant changes in chromatin organization. Heterochromatin is lost from the nuclear periphery and heterochromatic foci form within the nucleus. These foci are likely constitutive heterochromatin, given that they colocalize with H3K9me3 and HP1, but not H3K27me3.

The altered chromatin organization induced by LmnB1 OE is associated with differences in gene expression, but it is unclear what mediates these changes. Since there is no enrichment for specific biological pathways or transcription factor binding sites amongst the differentially expressed genes, it is possible that altered gene expression is a consequence of changes in chromatin accessibility or interactions. This will be tested using the Assay for Transposase-Accessible Chromatin with high throughput sequencing and Hi-C.

However, we also observed mislocalization of the heterochromatin marker, H3K9me3, by immunofluorescence imaging, suggesting that there may be differences in H3K9me3 deposition across the genome that correlate with gene expression. To analyze these changes, we used H3K9me3 antibodies to perform Cut&Run paired with next-generation sequencing, in cells overexpressing mCherry, mCherry-LmnB1, or mCherry-Lap2β. We are in the process of analyzing the data to identify differences, if any, in the sequences enriched for H3K9me3 upon LmnB1 OE, and will compare this with gene expression changes identified using mRNA-sequencing.

To elucidate how LmnB1 OE affects chromatin organization, we first assessed the dependence on chromatin re-organization after mitosis. We show that H3K9me3 marked heterochromatin still mislocalized away from the nuclear periphery in cells that cannot proceed through mitosis, suggesting that LmnB1 OE perturbs the tethering of heterochromatin at the

nuclear periphery. We did not observe any changes in the localization or expression of the proteome associated with the NE, including INM proteins and lamins. This shows the specificity of the phenotype for LmnB1, and suggests that its OE may be producing a physical barrier that perturbs the binding of heterochromatin at the NE.

These findings are distinct from other studies that correlate heterochromatin loss at the nuclear periphery with downregulation of INM proteins and LmnA (Solovei *et al.,* 2013; Lin and Fu, 2009). The most striking example is the inverted chromatin organization observed in LBR and LmnA null mice. These cells show heterochromatin loss from the nuclear periphery and their fusion into large chromocenters within the nucleoplasm (Solovei *et al.,* 2013). Although we did not observe fusion of the heterochromatin foci in our system, this study suggests the importance of LBR, LmnA, and their interacting partners as key factors in maintaining heterochromatin at the nuclear periphery. Given that we did not see any effects on the localization or expression of INM proteins and lamins, including LBR or LmnA, it is likely that their interacting partners are being disrupted upon LmnB1 OE. Some potential targets include HP1, PRR14, cKrox/Thpok, and Barrier-to-Autointegration Factor (BAF), which have all been shown to interact with INM proteins or lamins, and facilitate the binding of heterochromatin at the nuclear periphery (Poleshko *et al.,* 2013; Zullo *et al.,* 2012; Segurra-Toten *et al.,* 2002). We will therefore use our system to probe the interactions between these proteins and their binding partners at the nuclear envelope, to assess whether these may be disrupted and impacting the tethering of heterochromatin at the nuclear periphery.

We also assessed the effects of LmnB1 OE on cellular proliferation and senescence, and show that LmnB1 OE slows proliferation but does not induce senescence. These results agreed with previous studies demonstrating proliferation defects upon LmnB1 OE, but differed in regard

to the reversal of the proliferation defect with hTERT expression, and senescence induction (Barascu *et al.,* 2012; Dreesen *et al.,* 2013). Given the limited number of studies that have probed the effects of LmnB1 OE on cell proliferation, these differences may be attributed to inherent differences amongst the cell types used in each study (primary fibroblasts vs. immortalized epithelial cells). A better understanding of how LmnB1 OE affects cell proliferation and senescence will be important in resolving these results.

Altogether, the findings presented here demonstrate the pronounced effects of increased LmnB1 levels on chromatin organization and gene expression. Elucidating the mechanisms underlying these changes may provide insights into the development and progression of diseases with elevated expression of LmnB1, such as neurological diseases and cancer. Given that our cell lines are of epithelial origin, our results may have most relevance in the context of carcinomas, which are tumors that arise from epithelial cells. Although the changes in chromatin organization and gene expression may suggest a pro-tumorigenic role for LmnB1, we also observed a decrease in the proliferation rate of cells overexpressing LmnB1. Therefore, it will be important to further study this system to reconcile the effects observed upon LmnB1 OE.

Materials and Methods

Cell culture and drug treatments

RPE1 cells were cultured in DMEM/F12 with 10% fetal bovine serum, 1% penicillin-streptomycin, and 0.01 mg/mL hygromycin B. IMR90 cells were cultured in DMEM with 10% fetal bovine serum, 1% penicillin-streptomycin, 1% NEAA, and 1% glutaMAX.

RPE1 cells were arrested in G1/S phase using 3 uM aphidicolin for 24 hours. RPE1 cells were induced to senescence using 500 nM doxorubicin for 24 hours, washout with PBS, and collection at 10 days post doxorubicin pulse.

Plasmids and stable cell lines

The plasmids used in this chapter are listed in Table 4.1. The pLVXTP backbone was linearized using Not1 and EcoR1 restriction sites, and In-Fusion cloning was used to insert mCherry, or mCherry tagged LmnB1, LmnB1- ΔCaaX, or Lap2β. The pLVXTP plasmid was provided by Rusty Gage's lab.

Stable cell lines used in this chapter are listed in Table 4.2, and were produced according to the Addgene lentivirus production protocol using 293T cells. RPE1 and IMR90 cells were infected and selected with puromycin for 10 days. Clonal lines in RPE1 cells were established by isolating single cell clones in 96 well plates. Two clonal lines for each overexpression construct were utilized for downstream analyses. 0.05 ug/mL of doxycycline was used to induce overexpression of each construct.

Immunofluorescence imaging and analysis

Cells were grown on coverslips and fixed with 4% PFA in 1x PBS for 5 minutes at room temperature. Coverslips were blocked with IF buffer (10 mg/mL BSA, 0.1% Triton-X-100, 0.02% SDS, diluted in 1x PBS) for 20 minutes prior to incubation with primary and secondary antibodies diluted in IF buffer. The primary antibodies used are listed in Table 4.3. Coverslips were briefly incubated with Hoechst (1 ug/mL, Molecular Probes) and mounted with vectashield (Vector Labs). Imaging was performed on a Leica SP8 confocal microscope with a 63x 1.4NA oil immersion objective. Fiji was used to quantify fluorescence intensity of LmnB1 and generate plot profiles representing the colocalization of DNA foci and heterochromatin markers. LmnB1 fluorescence intensity values were normalized to the average fluorescence intensity observed in untreated cells.

Electron microscopy

Cultured cells were prepared for electron microscopy as previously reported (Lam *et al.,* 2015). Briefly, cells were cultured to approximately 70% confluence in 10 cm dishes. Media was gently poured out and ~1 mL of 2.5% glutaraldehyde in 100 mM cacodylate buffer with 3 mM $CaCl_2$ (cacodylate buffer) prewarmed to 37°C was gently added and swirled. Approximately 5 mL of ice cold fixative was gently added to the dish and cells were fixed on ice for 30 min. Cells were washed with ice cold cacodylate buffer three times before staining for 45 minutes with 1.5% osmium tetroxide reduced with 1.5% potassium ferrocyanide in cacodylate buffer at room temperature in the dark. Dishes were rinsed with ice cold water three times before cells were released from the dishes using cell scrapers and pelleted in Eppendorf tubes for further processing.

Cells pellets were stained with 1% uranyl acetate overnight at 4°C, and washed with ice cold water three times. Cells were serially dehydrated with changes of ice cold solutions of increasing ethanol concentrations, followed by two incubations for 45 minutes in anhydrous ethanol at room temperature. Cells were then infiltrated with Epon 812 (Electron Microscopy Sciences) and embedded in their Eppendorf tubes. Ultrathin sections (60 nm) were collected for each cell line using diamond knives (Diatome) on an ultramicrotome (Leica UC7), and imaging was performed on a Carl Zeiss Libra 120kV PLUS energy filtered transmission electron microscope.

mRNA-sequencing

RPE1 cells were treated with doxycycline for 24 hours and RNA was isolated using Trizol (Ambion) and purified with the RNeasy kit (Qiagen). RNA was shipped to Novogene for mRNA library preparation and run on the Illumina NovaSeq system (paired end 150). After quality check and trimming, sequencing data was aligned to the human reference sequence GRCh38 (hg38) and annotated with the corresponding gencode GTF file using the genome aligner STAR. The number of exonic reads per gene was calculated using featureCounts (from Rsubread package). After filtering out low expression genes, differential expression was assessed using DESeq2.

Cell proliferation and senescence assays

RPE1 cells ± doxycycline were cultured for 12 days, and the cumulative PDL was calculated. PDL = 3.32(log(total cells harvested/total cells seeded)). Doxycycline was added on Day 1. RPE1 cells were seeded into 12 wells with glass coverslips overnight, and incubated with

10 uM EdU for 24 hours. Coverslips were prepared according to the Click-IT EdU fluorescence detection protocol (Thermo Fisher Scientific). RPE1 cells were treated with doxycycline (9 days) or doxorubicin and seeded into ibidi 8 well chambers one day prior to senescence detection. The CellEvent senescence green detection kit was utilized and the chambers were prepared according to the manufacture's protocol (Thermo Fisher Scientific).

Western blotting

Cells were lysed in RIPA buffer (50 mM Tris-HCl pH 8, 150 mM NaCl, 1% Triton-X, 0.5% Sodium Deoxycholate, and 0.1% SDS) and protein concentration was normalized using the BCA protein assay (Thermo Fisher Scientific). Membranes were blocked using 5% nonfat milk in 1x TBST for 15 min prior to incubation with primary and secondary antibodies diluted in blocking buffer. The primary antibodies used are listed in Table 4.3. Secondary antibodies were conjugated to fluorescent dyes or HRP for detection.

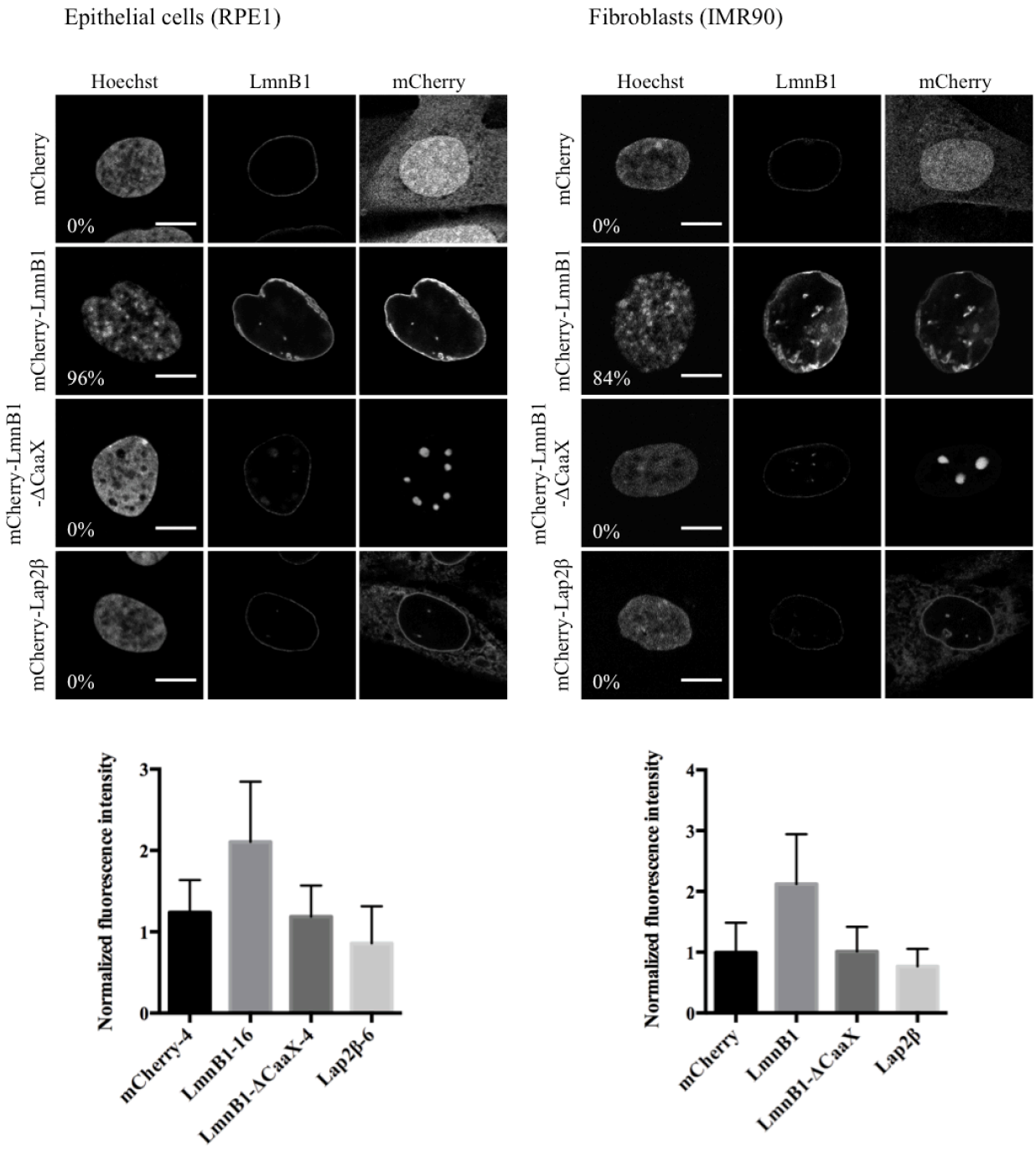

Figure 4.1. LmnB1 overexpression alters chromatin organization in epithelial cells and fibroblasts

Cells were treated with doxycycline for 24 hours and labeled with LmnB1. Confocal images of a single z slice through the center of the nucleus are shown. Scale bar is 10 μm. Percentages represent the number of cells exhibiting intranuclear DNA foci. Normalized fluorescence intensity of LmnB1 in each cell line is quantified at the bottom. Error bars indicate ± standard deviation.

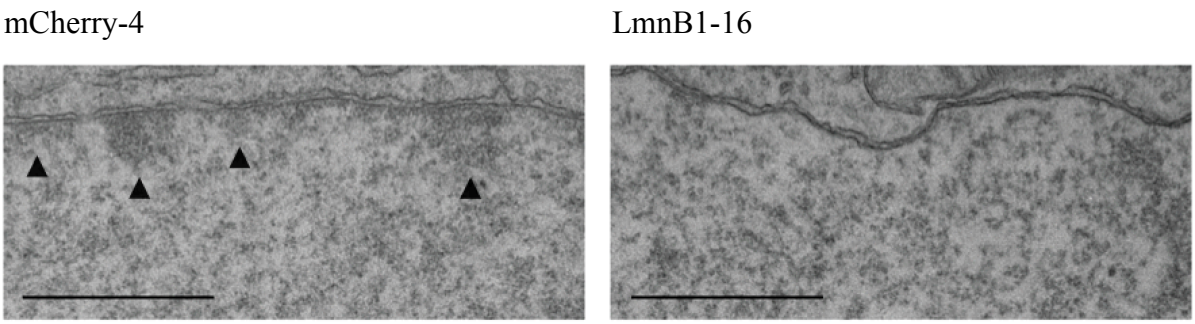

Figure 4.2. LmnB1 overexpression reduces heterochromatin at the nuclear periphery
Transmission electron microscopy images of RPE1 cells overexpressing mCherry or LmnB1. Cells were treated with doxycycline for 24 hours before processing and imaging. The nuclear envelope is at the top and the nucleus is at the bottom of each image. Arrowheads indicate heterochromatin lining the nuclear envelope. Scale bar is 1 μm.

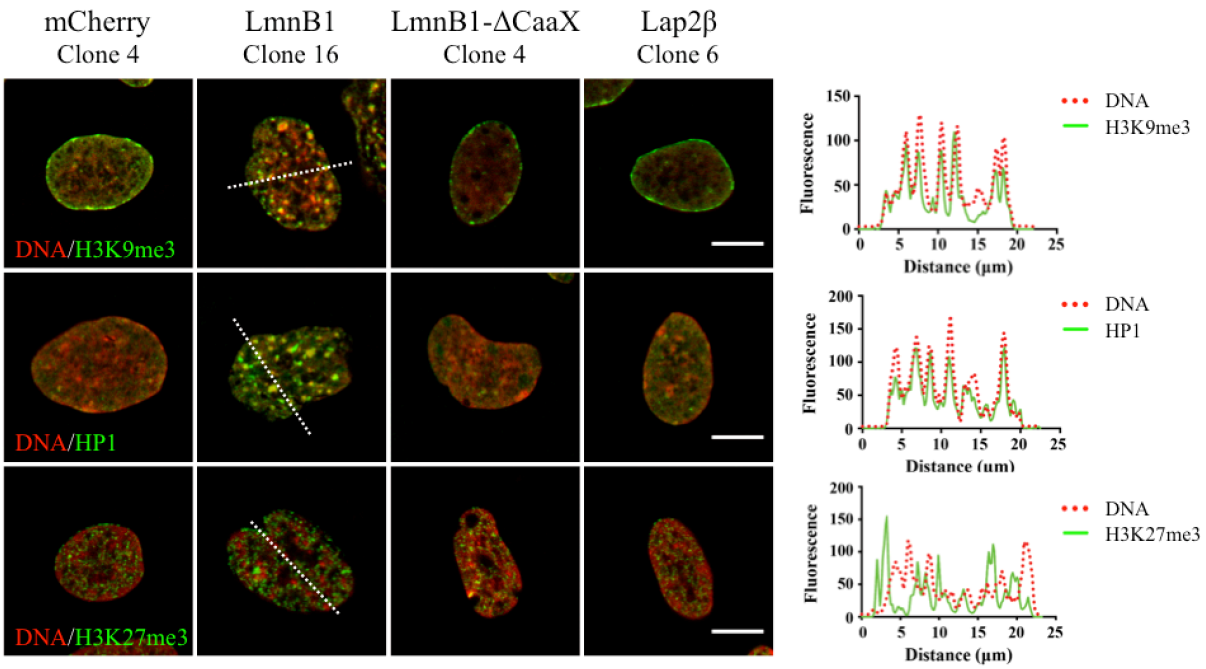

Figure 4.3. LmnB1 overexpression induced DNA foci colocalize with H3K9me3 and HP1, but not H3K27me3

Cells were treated with doxycycline for 24 hours and labeled with H3K9me3, HP1, or H3K27me3. Confocal images of a single z slice through the center of the nucleus are shown. Plot profiles illustrating the fluorescence signal of DNA and each heterochromatin marker over the dotted line are shown. Scale bar is 10 μm.

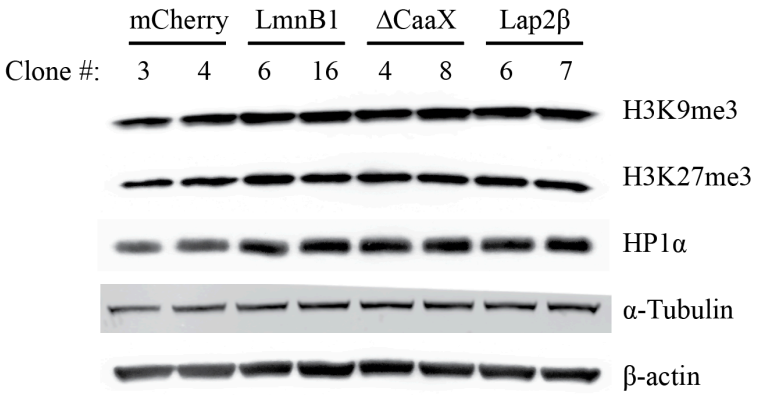

Figure 4.4. LmnB1 overexpression does not alter global expression of heterochromatin marks or heterochromatin binding proteins
Cells were treated with doxycycline for 24 hours and prepared for western blot analysis of H3K9me3, H3K27me3, and HP1α expression.

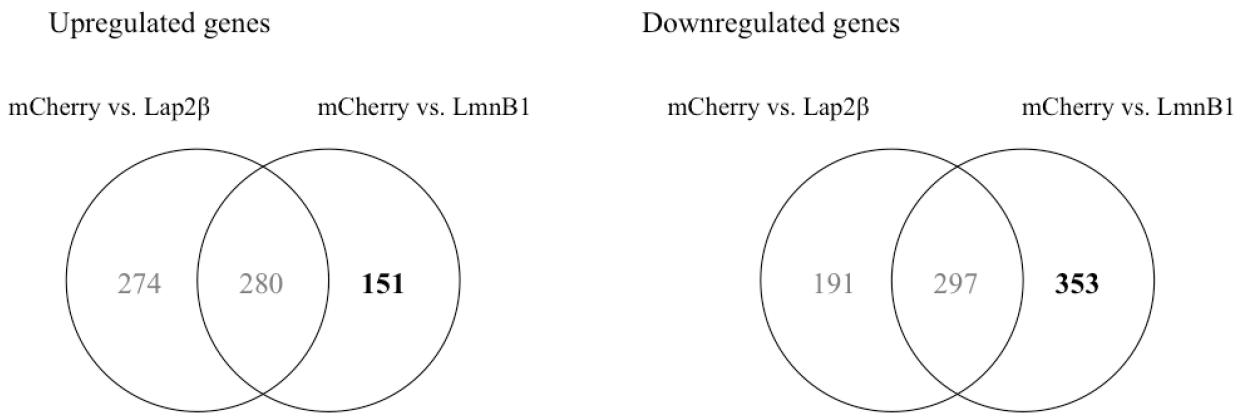

Figure 4.5. LmnB1 overexpression alters gene expression
RNA-sequencing was performed in RPE1 cells overexpressing mCherry, LmnB1, or Lap2β, at 24 hours post doxycycline induction. Differentially expressed genes were identified upon overexpression of LmnB1 and Lap2β when compared to mCherry overexpression. Comparison of these gene sets identified 151 genes specifically upregulated, and 353 genes specifically downregulated by LmnB1 overexpression.

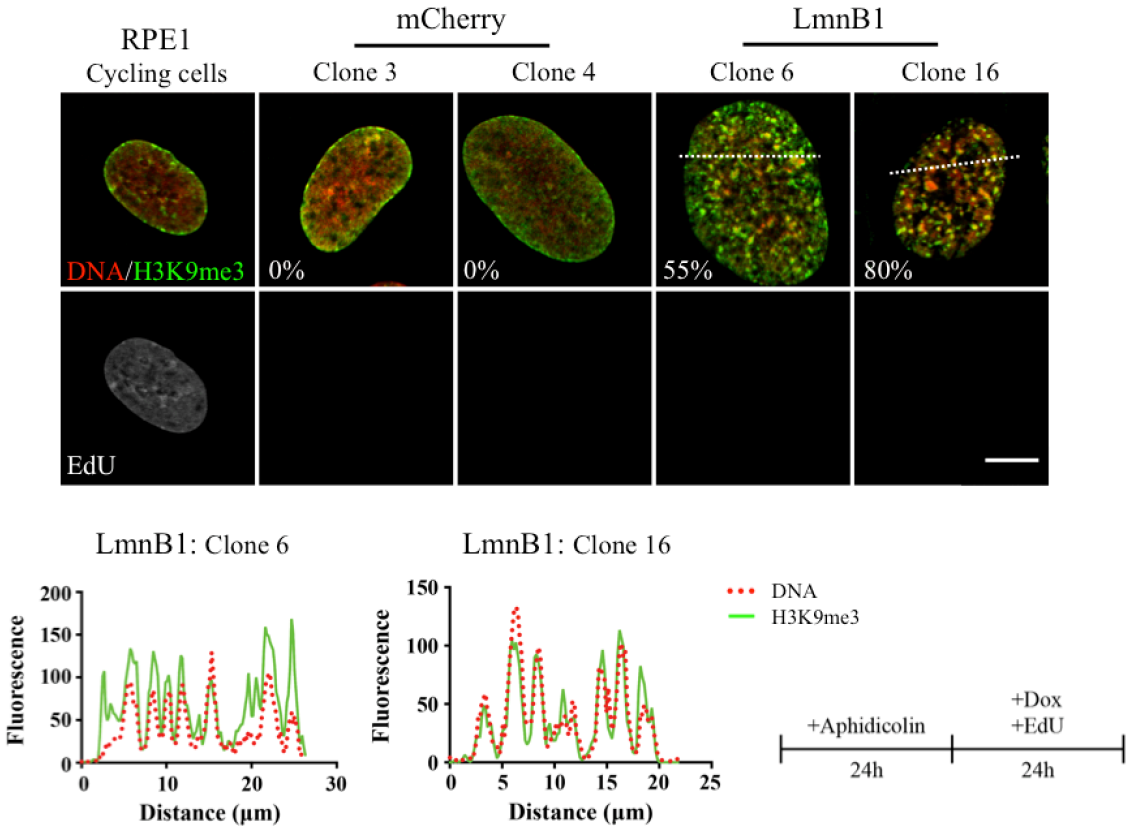

Figure 4.6. LmnB1 overexpression affects heterochromatin tethering at the nuclear envelope

Cells were arrested with aphidicolin (24 hours), followed by incubation with doxycycline and EdU (24 hours). Immunofluorescence imaging was used to analyze the localization of H3K9me3 and incorporation of EdU. Positive EdU detection in cycling RPE1 cells is shown. Confocal images represent a single z slice through the center of the nucleus. Plot profiles illustrating the fluorescence signal of DNA and H3K9me3 over the dotted line are shown. Scale bar is 10 µm.

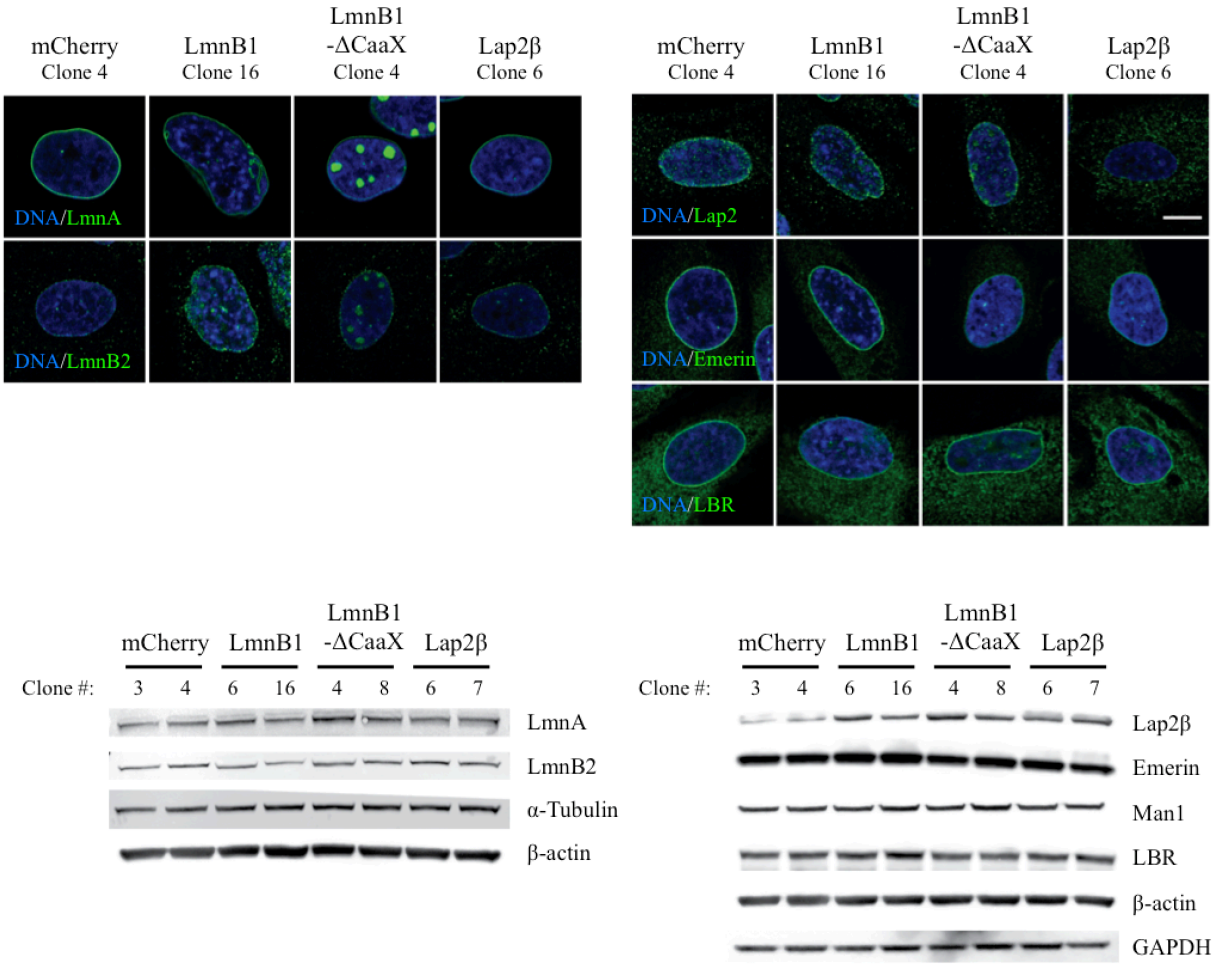

Figure 4.7. LmnB1 overexpression does not affect other lamin isoforms or INM proteins
The localization and expression of other lamin isoforms and INM proteins were analyzed by immunofluorescence imaging and western blot. Cells were treated with doxycycline for 24 hours. Confocal images of a single z slice through the center of the nucleus are shown. Scale bar is 10 μm.

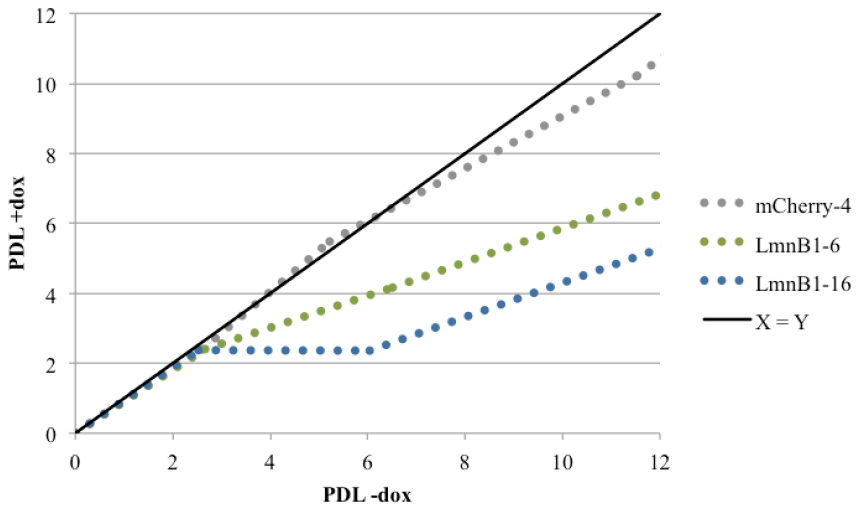

Figure 4.8. LmnB1 overexpression impairs cell proliferation
The cumulative population doubling level (PDL) for each cell line ±doxycycline was calculated on the same day, over 12 days. PDL = 3.32(log(total cells harvested/total cells seeded)). For each cell line, the PDL without doxycycline (X axis) is plotted against the PDL with doxycycline (Y axis). Doxycycline was added 24 hours after seeding (approximately 1 PDL).

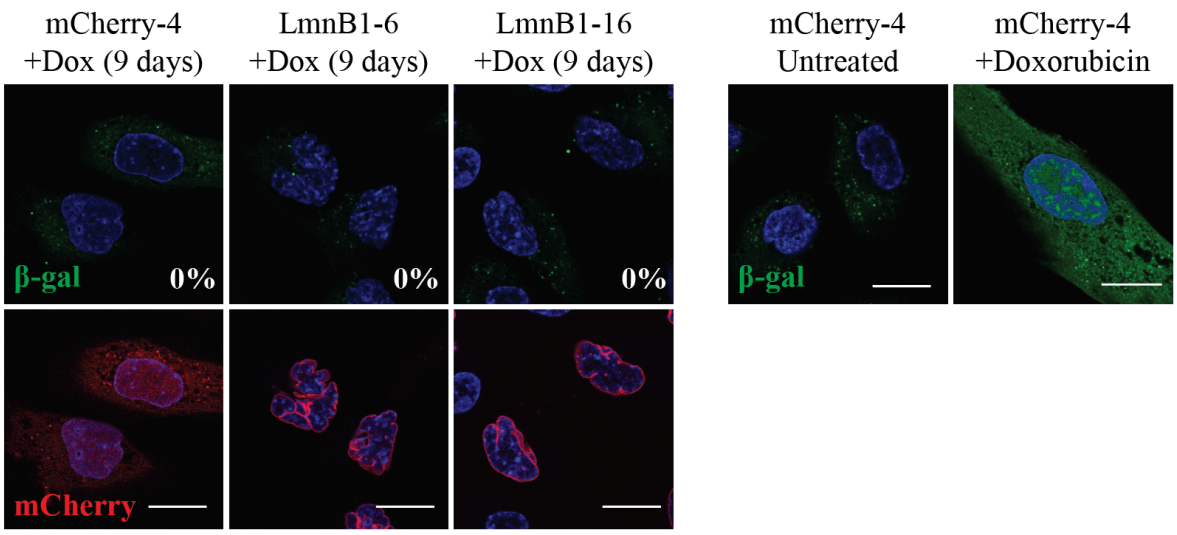

Figure 4.9. LmnB1 overexpression does not induce senescence
The CellEvent senescence green detection kit was used to detect senescence in cells treated with doxycycline for 9 days, or cells induced to senesce with doxorubicin. Confocal images of a single z slice through the center of the nucleus are shown. Scale bar is 20 μm.

Table 4.1. List of plasmids – Chapter 4

Plasmid name	Constitutive or inducible expression
pLVXTP mCherry	Inducible (Doxycyline, 0.05 ug/mL)
pLVXTP mCherry-LmnB1	Inducible (Doxycyline, 0.05 ug/mL)
pLVXTP mCherry-LmnB1-ΔCaaX	Inducible (Doxycyline, 0.05 ug/mL)
pLVXTP mCherry-Lap2β	Inducible (Doxycyline, 0.05 ug/mL)

Table 4.2. List of stable cell lines – Chapter 4

Parental cell line (plasmid)	Transfection or Infection (Selection)
RPE1 (pLVXTP mCherry)	Infection (Puromycin)
RPE1 (pLVXTP mCherry-LmnB1)	Infection (Puromycin)
RPE1 (pLVXTP mCherry-LmnB1-ΔCaaX)	Infection (Puromycin)
RPE1 (pLVXTP mCherry-Lap2β)	Infection (Puromycin)
IMR90 (pLVXTP mCherry)	Infection (Puromycin)
IMR90 (pLVXTP mCherry-LmnB1)	Infection (Puromycin)
IMR90 (pLVXTP mCherry-LmnB1-ΔCaaX)	Infection (Puromycin)
IMR90 (pLVXTP mCherry-Lap2β)	Infection (Puromycin)

Table 4.3. List of antibodies – Chapter 4

Antibody	Company	Dilution for IF	Dilution for WB
LmnA	Sigma-Aldrich, L1293	1:1000	1:1000
LmnB1	Santa Cruz Biotechnology, sc-56144	1:500	1:1000
LmnB2	Thermo Fisher Scientific, (LN43) #MA1-06104	1:200	1:1000
Emerin	Cell Signaling Technology, #30853	1:400	1:1000
Lap2	Santa Cruz Biotechnology, sc-28541	1:500	1:1000
LBR	Thermo Fisher Scientific, 12398-1-AP	1:100	1:1000
LEMD3 (Man1)	Thermo Fisher Scientific, TA500796		1:500
H3K9me3	Abcam, ab8898	1:500	1:1000
H3K27me3	Cell Signaling Technology, #9733	1:1600	1:1000
HP1α	Cell Signaling Technology, #2616	1:200	1:1000
HP1	Santa Cruz Biotechnology, sc-515341	1:200	
β-actin	Cell Signaling Technology, #3700		1:1000
α-Tubulin	Sigma Aldrich, T5168		1:5000
GAPDH	R&D Systems, MAB5718		1:5000

Acknowledgements

We thank Juliana S. Capitanio for help with RNA-sequencing and Cut&Run analysis; Novogene for mRNA library preparation and sequencing; the Salk Next Generation Sequencing core for sequencing Cut&Run libraries; and the Salk Waitt Advanced Biophotonics core, with funding from NIH-NCI CCSG: P30 014195, the Waitt Foundation, and the Chan-Zuckerberg Initiative Imaging Scientist Award, for electron microscopy sample preparation and imaging.

Chapter 4, in full, is currently being prepared for submission for publication. Kaneshiro, Jeanae M.; Capitanio, Juliana S.; Hetzer, Martin W. The dissertation author, under guidance of Martin W. Hetzer, was the primary researcher and author of this material.

References

Alcalá-Vida, R., Garcia-Forn, M., Castany-Pladevall, C., Creus-Muncunill, J., Ito, Y., Blanco, E., Golbano, A., Crespí-Vázquez, K., Parry, A., Slater, G., Samarajiwa, S., Peiró, S., Di Croce, L., Narita, M., & Pérez-Navarro, E. Neuron type-specific increase in lamin B1 contributes to nuclear dysfunction in Huntington's disease. *EMBO Mol Med.* **13**, e12105 (2021).

Barascu, A., Le Chalony, C., Pennarun, G., Genet, D., Imam, N., Lopez, B., & Bertrand, P. Oxidative stress induces an ATM-independent senescence pathway through p38 MAPK-mediated lamin B1 accumulation. *EMBO J.* **31**, 1080–1094 (2012).

Buchwalter, A., Kaneshiro, J. M., & Hetzer, M. W. Coaching from the sidelines: the nuclear periphery in genome regulation. *Nat Rev Genet.* **20**, 39–50 (2019).

Chandra, T., Ewels, P. A., Schoenfelder, S., Furlan-Magaril, M., Wingett, S. W., Kirschner, K., Thuret, J. Y., Andrews, S., Fraser, P., & Reik, W. Global reorganization of the nuclear landscape in senescent cells. *Cell Rep.* **10**, 471–483 (2015).

Di Micco, R., Sulli, G., Dobreva, M., Liontos, M., Botrugno, O. A., Gargiulo, G., dal Zuffo, R., Matti, V., d'Ario, G., Montani, E., Mercurio, C., Hahn, W. C., Gorgoulis, V., Minucci, S., & d'Adda di Fagagna, F. Interplay between oncogene-induced DNA damage response and heterochromatin in senescence and cancer. *Nat Cell Biol.* **13**, 292–302 (2011).

Dreesen, O., Chojnowski, A., Ong, P. F., Zhao, T. Y., Common, J. E., Lunny, D., Lane, E. B., Lee, S. J., Vardy, L. A., Stewart, C. L., & Colman, A. Lamin B1 fluctuations have differential effects on cellular proliferation and senescence. *J Cell Biol.* **200**, 605–617 (2013).

Freund, A., Laberge, R. M., Demaria, M., & Campisi, J. Lamin B1 loss is a senescence-associated biomarker. *Mol Biol Cell*. **23**, 2066–2075 (2012).

Goldman, R. D., Shumaker, D. K., Erdos, M. R., Eriksson, M., Goldman, A. E., Gordon, L. B., Gruenbaum, Y., Khuon, S., Mendez, M., Varga, R., & Collins, F. S. Accumulation of mutant lamin A causes progressive changes in nuclear architecture in Hutchinson-Gilford progeria syndrome. *Proc Natl Acad Sci USA*. **101**, 8963–8968 (2004).

Lam, S. S., Martell, J. D., Kamer, K. J., Deerinck, T. J., Ellisman, M. H., Mootha, V. K., & Ting, A. Y. Directed evolution of APEX2 for electron microscopy and proximity labeling. *Nat Methods*. **12**, 51–54 (2015).

Lin, S. T., & Fu, Y. H. miR-23 regulation of lamin B1 is crucial for oligodendrocyte development and myelination. *Dis Model Mech.* **2**, 178–188 (2009).

Malhas, A. N., Lee, C. F., & Vaux, D. J. Lamin B1 controls oxidative stress responses via Oct-1. *J Cell Biol.* **184**, 45–55 (2009).

McCord, R. P., Nazario-Toole, A., Zhang, H., Chines, P. S., Zhan, Y., Erdos, M. R., Collins, F. S., Dekker, J., & Cao, K. Correlated alterations in genome organization, histone methylation, and DNA-lamin A/C interactions in Hutchinson-Gilford progeria syndrome. *Genome Res*. **23**, 260–269 (2013).

Narita, M., Nũnez, S., Heard, E., Narita, M., Lin, A. W., Hearn, S. A., Spector, D. L., Hannon, G. J., & Lowe, S. W. Rb-mediated heterochromatin formation and silencing of E2F target genes during cellular senescence. *Cell.* **113**, 703–716 (2003).

Padiath, Q. S., Saigoh, K., Schiffmann, R., Asahara, H., Yamada, T., Koeppen, A., Hogan, K., Ptácek, L. J., & Fu, Y. H. Lamin B1 duplications cause autosomal dominant leukodystrophy. *Nat Genet.* **38**, 1114–1123 (2006).

Poleshko, A., Mansfield, K. M., Burlingame, C. C., Andrake, M. D., Shah, N. R., & Katz, R. A. The human protein PRR14 tethers heterochromatin to the nuclear lamina during interphase and mitotic exit. *Cell Rep.* **5**, 292–301 (2013).

Sadaie, M., Salama, R., Carroll, T., Tomimatsu, K., Chandra, T., Young, A. R., Narita, M., Pérez-Mancera, P. A., Bennett, D. C., Chong, H., Kimura, H., & Narita, M. Redistribution of the Lamin B1 genomic binding profile affects rearrangement of heterochromatic domains and SAHF formation during senescence. *Genes Dev.* **27**, 1800–1808 (2013).

Segura-Totten, M., Kowalski, A. K., Craigie, R., & Wilson, K. L. Barrier-to-autointegration factor: major roles in chromatin decondensation and nuclear assembly. *J Cell Biol.* **158**, 475–485 (2002).

Shah, P. P., Donahue, G., Otte, G. L., Capell, B. C., Nelson, D. M., Cao, K., Aggarwala, V., Cruickshanks, H. A., Rai, T. S., McBryan, T., Gregory, B. D., Adams, P. D., & Berger, S. L. Lamin B1 depletion in senescent cells triggers large-scale changes in gene expression and the chromatin landscape. *Genes Dev.* **27**, 1787–1799 (2013).

Shimi, T., Butin-Israeli, V., Adam, S. A., Hamanaka, R. B., Goldman, A. E., Lucas, C. A., Shumaker, D. K., Kosak, S. T., Chandel, N. S., & Goldman, R. D. The role of nuclear lamin B1 in cell proliferation and senescence. *Genes Dev*. **25**, 2579–2593 (2011).

Solovei, I., Kreysing, M., Lanctôt, C., Kösem, S., Peichl, L., Cremer, T., Guck, J., & Joffe, B. Nuclear architecture of rod photoreceptor cells adapts to vision in mammalian evolution. *Cell.* **137**, 356–368 (2009).

Solovei, I., Wang, A. S., Thanisch, K., Schmidt, C. S., Krebs, S., Zwerger, M., Cohen, T. V., Devys, D., Foisner, R., Peichl, L., Herrmann, H., Blum, H., Engelkamp, D., Stewart, C. L., Leonhardt, H., & Joffe, B. LBR and lamin A/C sequentially tether peripheral heterochromatin and inversely regulate differentiation. *Cell*. **152**, 584–598 (2013).

Sun, S., Xu, M. Z., Poon, R. T., Day, P. J., & Luk, J. M. Circulating Lamin B1 (LMNB1) biomarker detects early stages of liver cancer in patients. *J Proteome Res.* **9**, 70–78 (2010).

Yi, M., Li, T., Qin, S., Yu, S., Chu, Q., Li, A., & Wu, K. Identifying Tumorigenesis and Prognosis-Related Genes of Lung Adenocarcinoma: Based on Weighted Gene Coexpression Network Analysis. Biomed Res Int. **2020**, 4169691 (2020).

Zullo, J. M., Demarco, I. A., Piqué-Regi, R., Gaffney, D. J., Epstein, C. B., Spooner, C. J., Luperchio, T. R., Bernstein, B. E., Pritchard, J. K., Reddy, K. L., & Singh, H. DNA sequence-dependent compartmentalization and silencing of chromatin at the nuclear lamina. *Cell*. **149**, 1474–1487 (2012).